Structural and functional characterization of ice-binding proteins from cold-adapted fungi

(低温適応菌類由来氷結晶結合蛋白質の構造及び機能解析)

by Tatsuya Arai

A thesis submitted to the Division of Life Science,
Graduate School of Life Science, Hokkaido University
In conformity with the requirements for the degree of Doctor of Philosophy

Hokkaido University
Sapporo, Hokkaido, Japan
(March, 2019)

CONTENTS

List of Abbreviations

AFP	antifreeze protein
AFGP	antifreeze glycoprotein
AnpIBP	IBP from *Antarctomyces psychrotrophicus*
BMMY	buffered methanol-complex medium
BMGY	buffered glycerol-complex medium
CBB	Coomassie Brilliant Blue
CnIBP	IBP from *Chaetoceros neogracile*
ColIBP	IBP from *Colwellia* sp. strain SLW05
CfAFP	AFP from *Choristoneura fumiferana*
DAFP	AFP from *Dendroides canadensis*
FcIBP	IBP from *Fragilariopsis cylindrus*
FIPA	fluorescence-based ice plane affinity
FfIBP	IBP from *Flavobacterium frigoris* PS1.
GaIBP	IBP from *Glaciozyma antarctica* PI12
IBP	ice-binding protein
INP	ice nucleation protein
IAP	ice-affinity purification
I_h	unit structure of an ice crystal at 1 atmosphere
IBP	ice-binding protein
IBPv	IBP from a bacterium within the family Flavobacteriaceae (isolate 3519-10) in the Vostok Ice Core
IBS	ice-binding site
IPTG	isopropyl β-D-1-thiogalactopyranoside
KOD	DNA polymerase from *Thermococcus kodakarensis*
LpIBP	IBP from *Lolium perenne*
LeIBP	IBP from *Leucosporidium* sp. AY30
LB	Lysogeny Broth/Luria-Bertani
MpIBP	AFP from *Marinomonas primoryensis*
MD	molecular dynamics
Mw	molecular weight
NMR	Nuclear Magnetic Resonance
nfeAFP	type III AFP from notched-fin eelpout
NagIBP	IBP from *Navicula glaciei*

PBS	phosphate buffered-saline
RiAFP	AFP from *Rhagium inquisitor*
RMSD	root-mean-square deviation
SDS-PAGE	sodium dodecyl sulfate-polyacrylamide gel electrophoresis
sfAFP	AFP from snow flea
TH	thermal hysteresis
TisIBP	IBP from *Typhula ishikariensis*
T_f	freezing point
T_m	melting point
TmAFP	AFP from *Tenebrio molitor*
Tris	tris(hydroxymethyl)aminomethane
TE	Tris-EDTA buffer
YPDS	Yeast Extract Peptone Dextrose medium with Sorbitol

Chapter 1: General introduction

1.1. Living in cold environments

Our planet is a cold place where the temperature of almost 85% of soil and water environments is permanently or seasonally below 5°C [1]. Low temperature, together with other limiting factors including low water and nutrient availability, high osmotic pressure, and decrease of fluidity of the cell membrane, have a strong influence on organisms living in the cold-environments. Psychrophilic microorganisms have successfully colonized such extremely cold environments. These microorganisms take several cold-adaptation strategies such as formation of microbial communities in specific environments, increase of unsaturated lipids in the cell membrane, and production of cold-active enzymes [2].

Another problem for living in cold environments is formation of intra- and extra-cellular ice-crystals. Ice is a potentially lethal substance to a living organism. It can physically rupture a cell and alter the balance of water and dissolved ions within an organism. Psychrophilic microbes have evolved their survival strategies to inhabit ice-laden environments. They produce cryoprotectants to inhibit formation of intracellular and/or extracellular ice-crystals. Examples of the cryoprotective substances are polyalcohols and sugars [3, 4] that depress the freezing point of water in a colligative manner and ice-binding proteins (IBPs) that decrease the freezing point in a non-colligative way [5].

1.2. Ice-binding protein

Ice-binding proteins (IBPs) are ice-growth inhibitors produced by various kinds of cold-adapted species. IBPs were originally discovered in the serum of Antarctic fish over 40 years ago [6]. After that, they have been found in a variety of organisms including fish, insects, plants and microorganisms that inhabit ice-laden environments.

1.3. Thermal hysteresis

Binding of IBP to ice-crystal causes formation of micro-curvature between two adsorbed IBP molecules. This local growth is energetically unfavorable for water molecules to be incorporated into the ice-crystal due to the Kelvin effect. The further growth of ice is therefore restricted depending on the radius between adsorbed AFPs, resulting in a depression of the freezing point (T_f) in the solution due to the Gibbs-Thomson effect [7]. This is called adsorption inhibition mechanism and is a widely accepted mechanism for the all types of IBPs [8], while it does not mention how IBPs bind to ice-crystal. The difference between the melting point (T_m) and the

depressed T_f is referred to as thermal hysteresis (TH) and used as the indicator of the antifreeze activity (Fig. 1.1.).

The TH values are very different among IBP species. Based on TH activity, IBPs can be classified into two groups: moderate active and hyperactive groups [9]. The hyperactive IBPs are mainly identified from insects and they exhibit high TH activity of 2–6ºC at sub micromolar concentrations. Moderate IBPs are identified from fish and plants and shows TH activity of <1.5ºC at millimolar concentrations, while plant IBPs are weaker compared to fish IBPs. In the case of microbial IBPs, both hyperactive and moderate active ones are identified and their TH activities are very different (0.1~4°C).

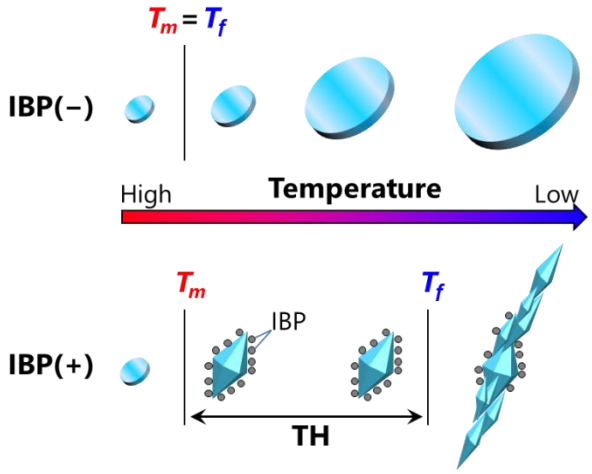

Fig. 1.1. Schematic representation of thermal hysteresis. Disc with blue color represent an ice-crystal. Diamond is IBP-bound ice-crystal. Gray sphere indicates an IBP molecule. IBP depresses *Tf* of the solution and makes difference between *Tf* and *Tm*. During TH gap, IBP modifies a single ice-crystal into a unique shape. Below *Tf*, the IBP-bound ice-crystal starts to grow suddenly, which is called ice-crystal "burst".

1.4. Ice-recrystallization inhibition (IRI)

Ice recrystallization (IR) is a process that large ice grains form at the expense of smaller ones due to Ostwald ripening process. IR occurs readily in a condition when the temperature fluctuates diurnally or during the freeze-thaw circle, which is just below the melting point. Generally, ice in nature forms as a multicrystalline mass. Boundaries between ice grains tend to be strained and unstable. At high sub-zero temperatures, an appreciable amount of liquid is present around the ice grains, and there is a tendency for

ice to recrystallize, resulting in a less total surface area of ice and an energetically favorable state.

Another function of IBPs is to inhibit this IR phenomenon [10]. Since IBPs coat surface of ice-crystals, they inhibit the both incorporation and desorption of water molecules (Fig.1.2.). IRI activity of IBP is also highly divergent, but it is not well understood what molecular property determines the strength of IRI.

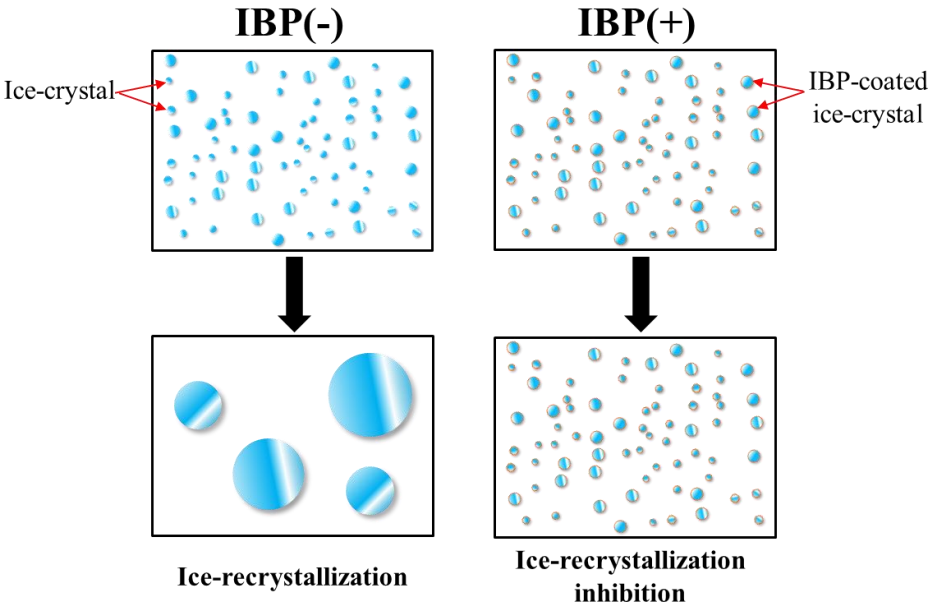

Fig. 1.2. Schematic representation of ice-recrystallization inhibition.

1.5. Physiological function

The variation in the strength of TH and IRI activities of IBPs is reflective of survival strategies of the host organisms. Generally, there are two strategies: freeze avoidance and freeze tolerance. Organisms that take the freeze-avoidance strategy such as fish and insects use IBPs to prevent ice-crystal growth, thus lowering the non-colligative freezing point of their body fluids [6, 11]. These organisms depend on relatively high TH activity where a greater freezing point depression is enough to encompass the temperature range of the environment. Thus, IBPs from these organisms are usually called as antifreeze proteins (AFPs).

Freeze tolerance is a strategy that involves minimizing inevitable frost damage to organisms [12, 13]. It is commonly associated with environments with high subzero temperature fluctuations and immobile organisms such as plants and some bacteria.

Freeze tolerant organisms produce IBPs to inhibit ice recrystallization and minimize the damage caused by it in frozen tissue and help themselves tolerate freeze rather than resist it. Therefore, these IBPs show weak TH activity but have effective IRI activity.

Microbes may use IBPs in different ways from the above organisms. Most of them secrete IBPs into the extracellular space possibly to keep water channels open in the surrounding ice so that the organism can respire, take up nutrients, and continue to live in that niche [14]. The mechanism of action of the IBPs could be either IR inhibition or TH, or both. Therefore, microorganisms might be doing on the outside what ice-challenged multicellular organisms do on the inside. If so, the secretion of IBPs would only be an efficient protective strategy if the proteins, needed at high concentrations, remained in the vicinity of the host cell or colony of cells, which would be the case if they were nearly surrounded by ice.

Another utilization of IBPs was proposed for two bacterial species is ice adhesion [15,16]. In these bacteria, IBPs anchor the host organisms to ice though a long linker on the cell membrane. The localization of the bacteria near the ice-water interface enables them to acquire much oxygen and nutrients.

1.6. Structure of IBP

The most interesting feature of IBPs is their surprising structural diversity (Fig. 1.3.). Currently tens of IBP structures are deposited in database. This incredible structural diversity of IBP is predicted to be a results of convergent evolution in different organisms [17].

1.6.1. Fish IBPs

Fish-derived AFPs can be categorized into five distinct groups (type I~IV AFPs, and antifreeze glycoprotein) based on their amino-acid sequences and structural properties. Type I AFPs is a 3-kDa alanine-rich alpha helical protein in which Thr residues are aligned with regular intervals on a protein surface [18, 19]. A hyperactive type I AFP (Maxi) folds as a long four-helix bundle [20]. Type II AFP is a 14-kDa globular protein composed of both alpha-helices and β-strands with five disulfide-bonds [21, 22]. Type III AFP is a 7-kDa globular protein with a compound ice-binding site, in which two adjacent IBSs are inclined at 150° to each other [23, 24]. Type IV AFP is thought to form a four helix bundle structure though its three-dimensional structure have not been determined yet [25]. AFGP is composed of 2-50 repetitive sequences (Ala-Ala-Thr) in which the side-chain of Thr is glycosylated with β-D-galactosyl (1,3)-α-N-acetyl-D-galactosamine [26].

1.6.2. Insect IBPs

IBPs from insect or terrestrial arthropods have been well characterized equally to those from fish. These IBPs shows a potent TH activity and known as hyperactive IBPs, reflecting their habitat environments in which they are exposed to harsh cold air temperature (<−30°C). The first IBP (TmAFP) from arthropods was documented in the yellow mealworm *T. molitor* [27]. This Thr- and Cys-rich IBP with a M.W. of 8.4 kDa exhibits TH up to 5.5°C and folds into a right-handed β-helix structure. TmAFP displays the Thr-X-Thr (T-X-T) pattern as the ice-binding site. Snow fleas are known to be a group of primitive arthropods where they prefer to live on the surface of snow [28]. One of them, *Hypogastrura harveyi*, displays a TH activity of 5.8°C in its body extract. The biochemical analyses revealed that the activity is derived from two types of AFP (sfAFP) isoforms with the Mw of 6.5 and 15.7 kDa, respectively. The X-ray structure of the small isoform has been determined, which showed that the protein is made up of six antiparallel left-handed polyproline II-like helices [29]. The longhorn beetle, Rhagium inquisitor, survives at a cold environment in the winter season of Siberia, which is due in part to the presence of an AFP (RiAFP). RiAFP, a 13 kDa molecule without isoforms, shows TH of around 6.5°C which is one of the highest measured among all AFP categories [30]. The X-ray crystal structure of RiAFP was reported, revealing its flat, silk-like β-helical (solenoid) structure [31].

1.6.3. Plant IBP

IBPs are also widely found in a range of over-wintering plants. As described in the above, freezing is unavoidable for plants during winter. These plants produce IBPs in intercellular spaces (apoplast), where it acts to minimize frost damage to the plant tissue largely through its IRI activity rather than TH activity. In fact, TH levels measured in freeze tolerant-plant IBPs are substantially lower than those obtained by freeze avoidant-animal IBPs, while the IRI activity exhibited by plant IBPs is typically higher than that of animal IBPs. Currently, two plant IBPs are characterized at the molecular level and summarized below.

A common vegetable, carrot (*Daucus carota*) produces an N-glycosylated, Leu-rich IBP (DcIBP) with a Mw of 36 kDa. DcIBP is composed of 24-amino acid tandem repeats [32, 33]. The 3D structural model of DcAFP has been proposed based on this repetitive feature, showing β-helical structure displaying conservative Asn residues on one side as it is predicted to be the ice-binding site (IBS). A forage grass, perennial ryegrass (*Lolium perenne*) produces a heat-stable IBP (LpIBP) composed of

118 amino acid residues with a M.W. of 11 kDa [34]. The X-ray crystal structure of LpIBP folds as a left-handed β-helical structure. LpIBP is currently the sole plant IBP whole structure is determined [35]. Although the high heat-stability of this protein is quite unusual, the mechanism is still remains to be investigated. The structure of LpIBP is very similar to insect IBPs, although the IBS of LpIBP lacks the regularity of insect IBPs.

1.6.4. Microbial IBP

Many cold-adapted microorganisms including bacteria [36], yeast [37], filamentous fungi [38], diatom [39], and copepod [40], produce IBP for various purposes. Most of microbial IBPs share a common structure unlike fish, insect, and plant IBPs. These IBPs are called IBP type I, IBP-I, or domain of unknown function (DUF) 3494 IBP. The structure of these IBPs is an irregularly stacked beta-helix with a neighboring alpha-helix [41,42]. Despite of their structural similarity, they do not have common-binding motif, resulting in different antifreeze activity. These differences may reflect their physiological role.

Another microbial IBP is identified from arctic bacterium *Marinomonas primoryensis*. MpIBP has a large beta-solenoid structure [43]. The structure of MpIBP is stabilized internal Ca^{2+}, so that this IBP exhibits antifreeze activity only in the presence of the ion. The IBS of this IBP have a unique binding-motif (Thr-X-Asx).

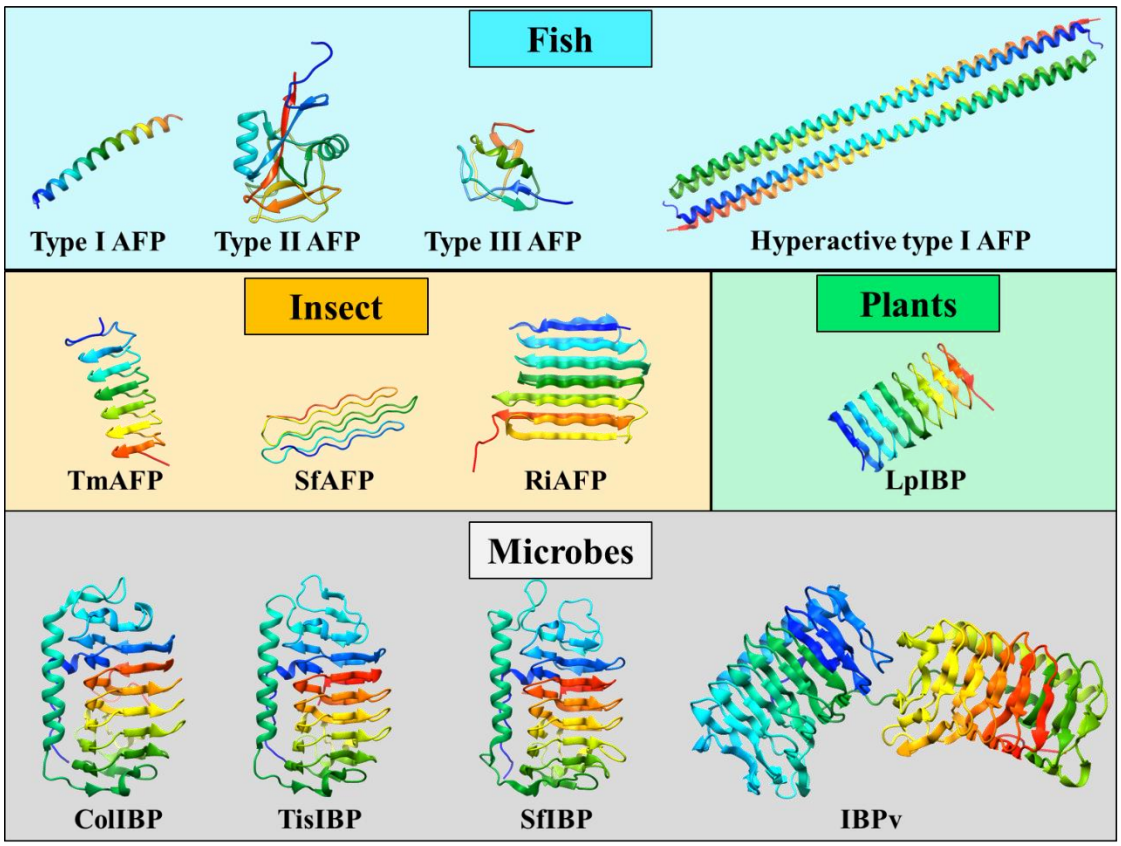

Figure 1.3. Crystal structures of ice-binding proteins. Type I AFP from winter flounder [Protein Data Bank (PDB) code: 1WFA. Type II AFP from longsnout poacher (PDB code: 2ZIB). (c) Type III AFP from ocean pout (PDB code: 1HG7). Hyperactive type I AFP (Maxi) from winter flounder (PDB code: 4KE2). TmAFP from the beetle, *Tenebrio molitor* (PDB code: 1EZG). RiAFP from the long beetle, *Rhagium inquisitor* (PDB code: 4DT5). sfAFP from snow flea (PDB code: 2PNE). LpIBP from perennial ryegrass, *Lolium perenne* (PDB code: 3ULT). ColIBP from an Antarctic sea ice bacterium, *Colwellia* sp. Strain SLW05 (PDB code: 3WP9). TisIBP from a snow mold fungus *Typhula ishilariensis* (PDB code: 5B5H). SfIBP from an Antarctic bacterium *Shewanella frigidimarina*. IBPv from a bacterium within the family Flavobacteriaceae (isolate 3519-10) in the Vostok Ice Core (PDB code: 5UYT). All structures are represented in cartoon and created by Chimera software.

1.7. Ice crystal

Ice is the solid state of water, in which water molecules are systematically arranged to construct a three-dimensional lattice (Fig. 1.4.). The ice crystal lattice denoted I_h is created under 1 atmospheric pressure, in which waters are arranged

hexagonally and characterized by three equivalent *a*-axes perpendicular to *c*-axis. The planes of ice are denoted with Miller-Bravais indices[44]. The planes perpendicular to *c*-axis are defined as basal plane. All planes parallel to *c*-axis are defined as prism planes, in which primary and secondary prism planes are typical target planes for many IBP species. Pyramidal planes cut the unit cell on angles.

Among such numerous planes, IBPs bind to specific planes. The binding of IBPs to specific ice planes results in the modification of a single ice crystal into unique morphologies, such as hexagonal plate, hexagonal bipyramid, and a lemon-like shape [45].

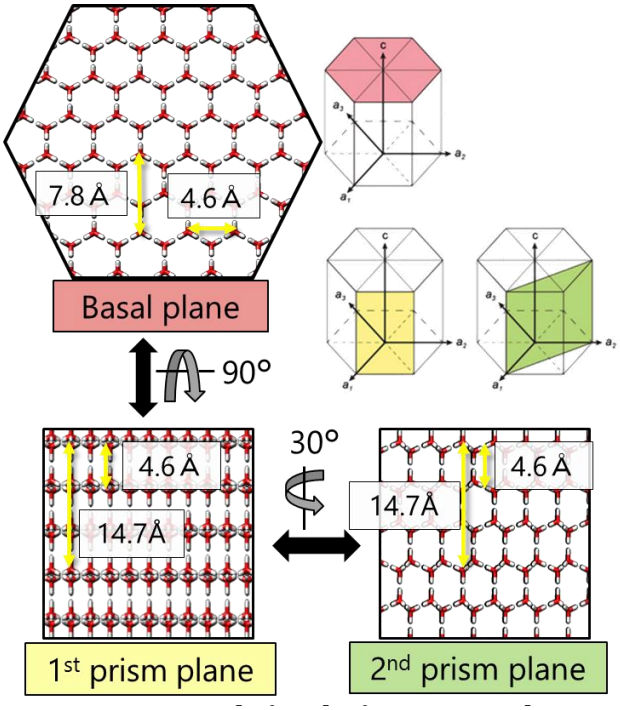

Figure 1.4. Structure of Ih ice.

1.8. Identification of IBP-bound planes

In 1991, Charles Knight experimentally demonstrated identification of planes of ice bound by IBP [46] . In this method, a macroscopic single ice crystal hemisphere on a brass cold finger was grown in IBP solution. In this process, IBP bound to the ice and became overgrown by microlayers of ice. Then, the hemisphere was allowed to sublime at -20°C for a few h to so that a protein residue where IBPs had bound would be visible as patches on the ice. Those patches could then be related to the Miller-Bravais indices to determine the planes of ice bound by the AFP. In 2014, this method was modified by et al. The modified method used fluorescent-tagged AFPs to

improve the ability to visualize the IBP-bound patches [47]. This method was named fluorescence-based ice plane affinity (FIPA) (Fig. 1.5.). The technique have identified target ice-planes of many IBPs.

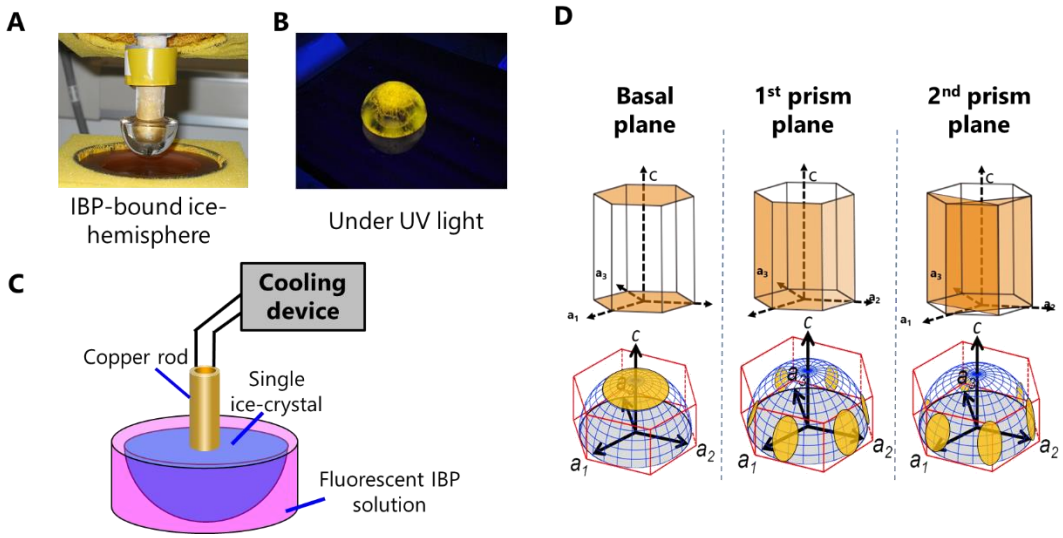

Figure 1.5. Schematic illustration of FIPA. (A) Photograph of IBP-bound hemisphere attached on a cold-finger. (B) Photograph of a UV-illuminated ice-hemisphere. (C) Schematic representation of FIPA. (D) Indication of IBP-bound planes on the hemisphere.

1.9. Molecular ice-binding mechanism

Proteins usually exhibit their own functions by adsorbing their specific ligands. Ligands of IBPs are specific ice-planes, although their binding-mechanism is still not completely understood because of difficulty of observing IBP-ice complex. The ice-binding site (IBS) of IBP is a relatively flat and hydrophobic region, and is supposed to organize the surface hydration waters into an ice-like arrangement [43]. These waters are thought to merge with the quasi-liquid layer constructing an ice-water interface at the edge of ice crystals, in which water molecules are well more ordered than those in bulk waters, but are disordered than the waters constructing ice lattice. When this semi-ordered water layer transitions to ice, the IBP would be frozen onto it through the ice-like surface waters that play an anchoring role. This is called “anchored clathrate water (ACW) mechanism” explaining the IBP’s ice-binding function, which was proposed based on the crystal structure of IBP from an Antarctic bacterium *Marinomonas primoryensis* (MpIBP) (Fig.1.6.). This IBP possesses extensive arrays of hydration waters that exhibited three dimensional space match with latticed waters

constructing basal- and primary prism ice crystal planes. However, such water networks were merely observed in the crystal structures of most of the other IBPs, since hydrophobic IBSs tend to be located in face-to-face by crystal-packing force, which is thought to displace water molecules around IBSs from their original positions [48]. It is, hence, still unclear whether this is the crucial ice-binding mechanism for all IBP species.

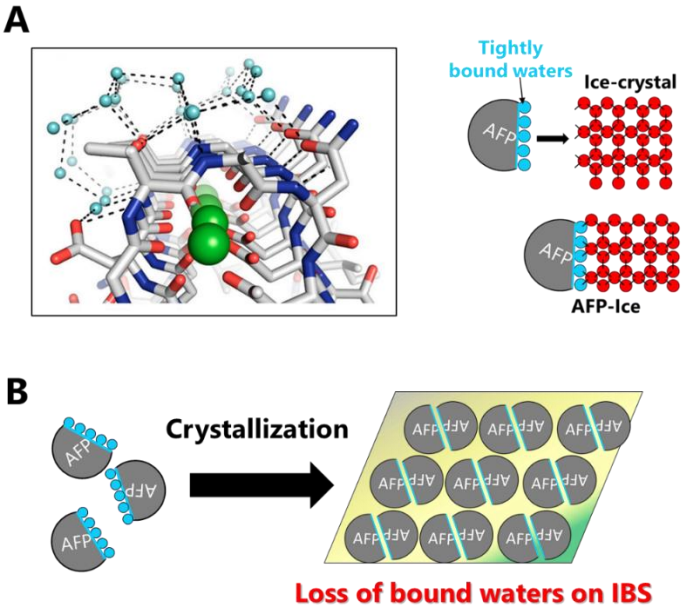

Fig. 1.6. Schematic illustration of anchored clathrate water mechanism. (A) Ice-like hydration waters on IBS of X-ray crystal structure of MpIBP. These waters are thought to anchor the protein with ice-crystal surface. (B) The ice-like waters are often lost during crystallization process for the structural analysis.

1.10. DUF3494 IBPs

As described above, DUF3494 IBPs are identified from many microbes living in cold. However, DUF3494 genes are identified not only from psychrophilic microbes but also from mesophilic ones. Currently characterized all DUF3494 sequences are from cold-adapted species. Therefore, it is still unknown whether the DUF3494 sequences from the non-cold-adapted microbes are IBP or not. Since DUF3494 IBSs do not have simple ice-binding motif, it is impossible to differentiate non-IBPs from the sequences. The first characterization of the DUF3494 sequence is reported in 2003 [38]. The authors identified the sequence from a snow mold fungus *Typhula ishikariensis*. After

that similar sequences are identified from sea-ice diatoms, bacteria, mushrooms, copepod, and yeasts.

Convergent evolution cannot explain the wide distribution of DUF3494 IBPs, because occurrence of the unusual structure of DUF3494 (Fig. 1.3.) in many different microbes is unlikely. Thus, the DUF3494 gene is thought to be passed through horizontal gene transfer (HGT): transmission of gene between two different organisms. HGT events readily occurs in niche environments in which non-adapted organisms are hard to survive, and HGT allows the receptor organism to colonize 'new' environments. It is reported that sea-ice environments are thought to be a "hot spot" for HGT [40], because Extracellular DNA in brine is highly concentrated compared to the under-ice ocean, which increases possibility of HGT at the solid-liquid interface than in the liquid phase. The high density of potential donor and recipient organisms within brine channels and the solid icy walls of the channels probably make of sea-ice a favorable environment for HGT.

Several approaches can be taken to detect HGT event. These include (i) detecting patchy phyletic distribution of a gene; (ii) identifying shared introns in the genes of unrelated species; (iii) identifying intronless genes in a species that is generally intron rich could indicate an acquisition from a bacterial source; (iv) finding similar genes shared among unrelated species that share a specific niche location. However, the most convincing method for identifying HGT is comparing phylogenetic trees of species and genes, in which disagreement between the species tree and the gene tree suggests occurrence of HGT. Using these approaches, several researchers showed occurrence of HGT of DUF3494 genes. Rainer Kiko [40] showed that IBPs from a dominant calanoid copepod *Stephos longipes* have high homology to DUF3494 IBPs from diatoms, bacteria and a snow mold and, in contrast, no homologs in any metazoan lineage, and he proposed possibility that the copepod proteins were obtained through HGT. Maddalena Bayer-Giraldi et al. [49] also showed that sea-ice diatom *Fragilariopsis* IBPs are more related to fungal and bacterial sequences, whereas *Navicula glaciei* and *Chaetoceros neogracile* sequences are phylogenetically closer to Archaea than to other diatoms, indicating that these diatoms acquired the IBP genes from different ancestors. From these results, they concluded a high mobility of DUF3494 IBP genes and underline their importance for polar organisms. James A. Raymond [50] reported that phylogenetic trees based on the sequences of IBPs and 18S rRNA of diatom/algal are not resemble, and all of sea ice diatoms examined so far show IBP activity, while mesophilic diatoms examined so far do not show IBP activity. Since

it is unlikely that all of the mesophilic diatoms have lost the DUF3494 gene, he concluded occurrence of HGT of IBP gene in these diatom/algae.

1.11. Fungal IBPs

The kingdom Fungi includes about 140,000 species such as yeasts, rusts, mildews, molds, mushrooms. Fungi are among the most widely distributed organisms on Earth. The enormous capability of fungi to cope with and survive various environments has been focused for years.

Ascomycota and basidiomycota are the first and second largest phylum of fungi, respectively. Both ascomycete and basidiomycete species inhabit extremely cold environments including Arctic and Antarctic regions. The psychrophilic fungi should have ability to adapt to low temperature and at least some of them should produce IBPs. Indeed, many basidiomycetes are reported to produce DUF3494 IBPs (,,,,). On the other hand, IBP-producing ascomycetes are currently limited. Nan Xiao et al. performed assays of antifreeze activity against culture media of a total of 23 psychrophilic ascomycetes, but found that only two species (*Antarctomyces psychrotrophicus* and *Penicillium camembertii*) produce ice-shaping substances [51]. In their study, only the former was confirmed to produce ice-binding "protein", while the later was not. A question arises from this study – is the number of IBP-producing ascomycete actually small? In the NCBI database, there are tens of DUF3494 IBP-like sequences from ascomycetes, so that it is likely that ascomycete IBPs are just not identified (or studied). Since none of these ascomycete IBP-like sequences have been characterized, it is unknown whether they are actually IBP or not.

1.12. Purpose and Scope of this dissertation

An ascomycete *Antarctomyces psychrotrophicus* is one of the dominant ascomycetes in Antarctica and is isolated from several different substrates in Antarctica, such as soils, waters in lakes, marine macroalgae, that are exposed to freeze-thaw cycles. This species is currently the sole ascomycete that is confirmed to produce IBP (AnpIBP). AnpIBP is a glycosylated IBP with a molecular weight of < 28 kDa and is secreted into extracellular space. AnpIBP shows moderate TH and effective IRI activities. However, its primary-tertiary structure is not revealed. Is AnpIBP similar to other fungal IBPs (DUF3494) species? If this IBP is similar to other fungal IBPs (DUF3494 IBPs), it is highly possible that the other sequence found in ascomycetes are also IBP. Because of lack of knowledge about ascomycete IBPs, it is not well understood how these IBPs work in the physiological conditions.

The main focus on my thesis is biophysical, evolutional, and structural characterization of AnpIBP. Since AnpIBP is currently the sole IBP that is isolated from ascomycete, it was a good example to shed light on the physiological role, evolutionary history, and ice-binding mechanism of ascomycete IBP. We identified cDNA sequences of AnpIBP and recombinantly expressed and characterized one of the AnpIBP isoform. And also, we performed phylogenetic analysis of AnpIBP as well as other putative ascomycete IBPs.

Reference

1. Herbert, R.A. (1986). The Ecology and physiology of psychrophilic microorganisms. In Microbes in Extreme Environments (Herbert, R.A. & Codd, G.A., eds.) pp. 1-23, Academic Press. London, England.
2. Wang M, Tian J, Xiang M, & Liu X (2017) Living strategy of cold-adapted fungi with the reference to several representative species. *Mycology* **8**, 178–188.
3. Su Y, Jiang X, Wu W, Wang M, Hamid MI, Xiang M & Liu X (2016) Genomic, transcriptomic, and proteomic analysis provide insights into the cold adaptation mechanism of the obligate psychrophilic fungus *Mrakia psychrophila*. *G3 Bethesda* 6, 3603–3613.
4. Phadtare S (2004) Recent developments in bacterial cold-shock response. *Curr Issues Mol Biol* 6, 125-136.
5. Davies PL (2014) Ice-binding proteins: a remarkable diversity of structures for stopping and starting ice growth. *Trends Biochem Sci* 39, 548–555.
6. DeVries, A. L. and Wohlschlag, D. E. (1969) Freezing resistance in some Antarctic fishes. *Science* 163, 1073-1075.
7. Knight, C. A., Cheng, C. C. and DeVries, A. L. (1991) Adsorption of α-helical antifreeze peptides on specific ice crystal surface planes. *Biophys. J.* 59, 409-418.
8. Raymond, J. A. and DeVries, A. L. (1977) Adsorption inhibition as a mechanism of freeze resistance in polar fishes. *Proc. Natl. Acad. Sci. U.S.A.* 74, 2589-2593.
9. Scotter, A.J., Marshall, C.B., Graham, L.A., Gilbert, J.A., Garnham, C.P. and Davies, P.L. (2006). The basis for hyperactivity of antifreeze proteins. *Cryobiology* 53, 229-239.
10. Knight, C.A., Wen, D. and Laursen, R.A. (1995) Nonequilibrium antifreeze peptides and the recrystallization of ice. *Cryobiology* 32, 23-34.

11. Graether, S.P., Kuiper, M.J., Gagné, S.M., Walker, V.K., Jia, Z., Sykes, B.D., and Davies, P.L. (2000) Beta-helix structure and ice-binding properties of a hyperactive antifreeze protein from an insect. *Nature* 406, 325-328.
12. Duman, J. and Olsen, T.M. (1993) Thermal hysteresis protein activity in bacteria, fungi and phylogenetically diverse plants. *Cryobiology* 30, 322–328.
13. Smallwood, M. et al. (1999) Isolation and characterization of a novel antifreeze protein from carrot (*Daucus carota*). *Biochem. J.* 340, 385–391.
14. Raymond, J.A. (2011) Algal ice-binding proteins change the structure of sea ice. *Proc. Natl. Acad. Sci .U.S.A.* 108, E198.
15. Guo, S. et al. (2012) Re-evaluation of a bacterial antifreeze protein as an adhesin with ice-binding activity. *PLoS ONE* 7, e48805.
16. Vance, T. D., Graham, L. A., & Davies, P. L. (2018). An ice-binding and tandem beta-sandwich domain-containing protein in Shewanella frigidimarina is a potential new type of ice adhesin. *FEBS J, 285*, 1511-1527.
17. Chen, L. et al. (1997) Convergent evolution of antifreeze glycoproteins in Antarctic notothenioid fish and Arctic cod. *Proc. Natl. Acad. Sci.* U.S.A. 94, 3817–3822.
18. Yang, D. S., Sax, M., Chakrabartty, A. and Hew, C. L. (1988) Crystal structure of an antifreeze polypeptide and its mechanistic implications. *Nature* 333, 232-237.
19. Sicheri, F., and Yang, D. S. (1995) Ice-binding structure and mechanism of an antifreeze protein from winter flounder. *Nature* 375, 427-431.
20. Sun, T., Lin, F. H., Campbell, R. L., Allingham, J. S. and Davies, P. L. (2014) An antifreeze protein folds with an interior network of more than 400 semi-clathrate waters. *Science* 343, 795-798.
21. Gronwald, W., Loewen, M. C., Lix, B., Daugulis, A. J., Sönnichsen, F. D., Davies, P. L. and Sykes, B. D. (1998) The solution structure of type II antifreeze protein reveals a new member of the lectin family. *Biochemistry* 37, 4712-4721.
22. Nishimiya, Y., Kondo, H., Takamichi, M., Sugimoto, H., Suzuki, M., Miura, A. and Tsuda, S. (2008) Crystal structure and mutational analysis of Ca2+ -independent type II antifreeze protein from longsnout poacher, *Brachyopsis rostratus. J. Mol. Biol.* 382, 734-746.
23. Sönnichsen, F. D., Sykes, B. D., Chao, H. and Davies, P. L. (1993) The nonhelical structure of antifreeze protein type III. *Science* 259, 1154-1157.
24. Sönnichsen, F. D., DeLuca, C. I., Davies, P. L. and Sykes, B. D. (1996) Refined solution structure of type III antifreeze protein: hydrophobic groups may be involved in the energetics of the protein–ice interaction. *Structure* 4, 1325-1337.

25. Deng, G., Andrews, D. W. and Laursen, R. A. (1997) Amino acid sequence of a new type of antifreeze protein, from the longhorn sculpin *Myoxocephalus octodecimspinosis*. *FEBS Lett*. 402, 17-20.
26. Cheng, C. H. C. and Chen, L. (1999) Evolution of an antifreeze glycoprotein. *Nature* 401, 443-444.
27. Liou, Y. C., Tocilj, A., Davies, P. L. and Jia, Z. (2000) Mimicry of ice structure by surface hydroxyls and water of a β-helix antifreeze protein. Nature 406, 322-324.
28. Pentelute, B. L., Gates, Z. P., Tereshko, V., Dashnau, J. L., Vanderkooi, J. M., Kossiakoff, A. A. and Kent, S. B. (2008) X-ray structure of snow flea antifreeze protein determined by racemic crystallization of synthetic protein enantiomers. J. Am. Chem. Soc. 130, 9695-9701.
29. Mok, Y. F., Lin, F. H., Graham, L. A., Celik, Y., Braslavsky, I. and Davies, P. L. (2010) Structural basis for the superior activity of the large isoform of snow flea antifreeze protein. Biochemistry 49, 2593-2603.
30. Zachariassen, K. E., Li, N. G., Laugsand, A. E., Kristiansen, E. and Pedersen, S. A. (2008) Is the strategy for cold hardiness in insects determined by their water balance? A study on two closely related families of beetles: Cerambycidae and Chrysomelidae. J. Comp. Physiol. B 178, 977-984.
31. Hakim, A., Nguyen, J. B., Basu, K., Zhu, D. F., Thakral, D., Davies, P. L., Isaacs, F. J., Modis, Y. and Meng, W. (2013) Crystal structure of an insect antifreeze protein and its implications for ice binding. J. Biol. Chem. 288, 12295-12304.
32. Worrall, D., Elias, L., Ashford, D., Smallwood, M., Sidebottom, C., Lillford, P., Telford, J., Holt, C. and Bowles, D. (1998) A carrot leucine-rich-repeat protein that inhibits ice recrystallization. Science 282, 115-117.
33. Smallwood, M., Worrall, D., Byass, L., Elias, L., Ashford, D., Doucet, C. J., Holt, C., Telford, J., Lillford, P. and Bowles, D. J. (1999) Isolation and characterization of a novel antifreeze protein from carrot (*Daucus carota*). Biochem. J. 340, 385-391.
34. Sidebottom, C., Buckley, S., Pudney, P., Twigg, S., Jarman, C., Holt, C., Telford, J., MaArthur, A., Worrall, D., Hubbard, R. and Lillford, P. (2000) Heat-stable antifreeze protein from grass. Nature 406, 256.
35. Middleton, A. J., Marshall, C. B., Faucher, F., Bar-Dolev, M., Braslavsky, I., Campbell, R. L., Walker, V. K. and Davies, P. L. (2012) Antifreeze protein from freeze-tolerant grass has a beta-roll fold with an irregularly structured ice-binding site. J. Mol. Biol. 416, 713-724.
36. Raymond J. A., Fritsen, C., and Shen, K. (2007) An ice-binding protein from an Antarctic sea ice bacterium. FEMS Microbiol Ecol 61, 214-221.

37. Lee, J. K., Park, K. S., Park, S., Park, H., Song, Y. H., Kang, S., et al. (2010) An extracellular ice-binding glycoprotein from an Arctic psychrophilic yeast. Cryobiology 60, 222-228
38. Hoshino, T., Kiriaki, M., Ohgiya, S., Fujiwara, M., Kondo, H., Nishimiya, Y., Yumoto, I., and Tsuda, S. (2003) Antifreeze proteins from snow mold fungi. Can J Bot 81, 1175-1181.
39. Janech, M. G., Krell, A., Mock, T., Kang, J. S., and Raymond, J. A. (2006) Ice-binding protein from sea ice diatoms. J phycol 42, 410-416.
40. Kiko, R. (2010) Acquisition of freeze protection in a sea-ice crustacean through horizontal gene transfer? Polar Biol 33, 543–556.
41. Lee, J. H., Park, A. K., Do, H., Park, K. S., Moh, S. H., Chi, Y. M., et al. (2012) Structural basis for antifreeze activity of ice-binding protein from arctic yeast. J Biol Chem 287, 11460-11468.
42. Kondo, H., Hanada, Y., Sugimoto, H., Hoshino, T., Garnham, C. P., Davies, P. L. and Tsuda, S. (2012) Ice-binding site of snow mold fungus antifreeze protein deviates from structural regularity and high conservation. Proc. Natl. Acad. Sci. U.S.A. 109, 9360-9365.
43. Garnham, C. P., Campbell, R. L. and Davies, P. L. (2011) Anchored clathrate waters bind antifreeze proteins to ice. Proc. Natl. Acad. Sci. U.S.A. 108, 7363-7367.
44. Hobbs PV (1974) Ice physics (Clarendon Press, Oxford) p 837.
45. Scotter, A. J., Marshall, C. B., Graham, L. A., Gilbert, J. A., Garnham, C. P. and Davies, P. L. (2006) The basis for hyperactivity of antifreeze proteins. Cryobiology 53, 229-239.
46. Knight, C. A., Cheng, C. C. and DeVries, A. L. (1991) Adsorption of α-helical antifreeze peptides on specific ice crystal surface planes. Biophys. J. 59, 409-418.
47. Basu, K., Garnham, C.P., Nishimiya, Y., Tsuda, S., Braslavsky, I., and Davies, P.L. (2014) Determining the ice-binding planes of antifreeze proteins by fluorescence-based ice plane affinity. J. Vis. Exp. 15, e51185.
48. Sun, T., Gauthier, S. Y., Campbell, R. L. and Davies, P. L. (2015) Revealing Surface Waters on an Antifreeze Protein by Fusion Protein Crystallography Combined with Molecular Dynamic Simulations. J. Phys. Chem. B 119, 12808-12815.
49. Bayer-Giraldi M, Uhlig C, John U, Mock T & Valentin K (2010) Antifreeze proteins in polar sea ice diatoms: diversity and gene expression in the genus *Fragilariopsis*. *Environ Microbiol* **12**, 1041–1052.
50. Raymond JA & Kim HJ (2012) Possible role of horizontal gene transfer in the colonization of sea ice by algae. *PloS one* **7**, e35968.

51. Xiao N, Suzuki K, Nishimiya Y, Kondo H, Miura A, Tsuda S & Hoshino T (2010) Comparison of functional properties of two fungal antifreeze proteins from *Antarctomyces psychrotrophicus* and *Typhula ishikariensis*. *FEBS J* **277**, 394–403.

Chapter 2: Functional and evolutionary characterization of AnpIBP

Preface: This chapter was published in the FEBS Journal: Arai, T., Fukami D., Hoshino T., Kondo, H. and Tsuda, S. (2018) Ice-binding proteins from the fungus Antarctomyces psychrotrophicus possibly originate from two different bacteria through horizontal gene transfer.

2.1. Abstract

Various microbes, including fungi and bacteria, that live in cold environments produce ice-binding proteins (IBPs) that protect them from freezing. Ascomycota and Basidiomycota are two major phyla of fungi, and *Antarctomyces psychrotrophicus* is currently designated as the sole ascomycete that produces IBP (AnpIBP). However, its complete amino acid sequence, ice-binding property, and evolutionary history have not yet been clarified. Here, we determined the peptide sequences of three new AnpIBP isoforms by total cDNA analysis and compared them with those of other microbial IBPs. The AnpIBP isoforms and ascomycete-putative IBPs were found to be phylogenetically close to the bacterial ones but far from the basidiomycete ones, which is supported by the higher sequence identities to bacterial IBPs than basidiomycete IBPs, although ascomycetes are phylogenetically distant from bacteria. In addition, two of the isoforms of AnpIBP share low sequence identity and are not close in the phylogenetic tree. It is hence presumable that these two AnpIBP isoforms were independently acquired from different bacteria through horizontal gene transfer (HGT), which implies that ascomycetes and bacteria frequently exchange their IBP genes. The non-colligative freezing-point depression ability of AnpIBP was not very high, whereas it exhibited significant abilities of ice-recrystallization inhibition, ice shaping, and cryo-protection against freeze-thaw cycles even at submicromolar concentrations. These results suggest that HGT is crucial for the cold-adaptive evolution of ascomycetes, and their IBPs offer freeze resistance to organisms to enable them to inhabit the icy environments of Antarctica.

2.2. Introduction

Microbes that adapt to low temperatures (or psychrophiles) can inhabit extremely cold environments, such as the Arctic and Antarctic regions[1,2]. These microbes have acquired several strategies against freezing that inevitably accompany ice crystal formation and overcome physical damages. An example of such a strategy is the production of cryoprotective substances, such as glycerol[3], trehalose[4], and ice-binding proteins (IBPs)[5], which inhibit ice crystal growth. Nevertheless, cold-survival mechanism and phylogenetic relationship of microbial IBPs, especially in fungi, are not well understood.

Biophysical studies have revealed that IBPs bind to specific planes of ice crystals to arrest further growth, which contributes to the survival of host organisms in icy environments[6]. One of the principle functions of IBPs is to inhibit ice recrystallization (IR)[7], a phenomenon of larger ice crystal formation at the expense of smaller ones that causes freezing damages to cells and tissues. IBPs can also modify the shape of ice crystals to mitigate their harsh texture around microbes[8]. In some animals that have naturally high (mg ml^{-1}) IBP concentrations, IBPs also cause the non-colligative freezing-point depression termed thermal hysteresis (TH)[9]. Although microbial IBPs are thought to exist at μg/ml concentrations in the extracellular space, they can exhibit TH when they are concentrated in the laboratory.

Various types of cold-adapted microbes, including bacteria[10], yeast[11], mushroom[2], algae[8], and a copepod[13], are known to produce IBPs. Most of these microbial IBPs share a common sequence called the “domain of unknown function (DUF) 3494,” which comprises approximately 190 amino acid residues exhibiting 30%–70% sequence identities. X-ray crystallographic studies have shown that these IBPs are commonly folded into an irregular beta-helical structure accompanying one long alpha-helix[14].

Ascomycetes and basidiomycetes are two major lineages of fungi and are closely related to each other. In the NCBI database (http://www.ncbi.nlm.nih.gov/), over 200 species of fungal DUF3494 sequences have been deposited, half of which is derived from ascomycetes and the other half from basidiomycetes. Since DUF3494s have been identified from microorganisms that live in both cold and non-cold regions, not all of them may be IBPs. So far none of the ascomycete-derived proteins containing a DUF3494 sequence has been examined for ice-binding activity, whereas the activity was observed for various IBPs from basidiomycetes[11,12,15].

Horizontal gene transfer (HGT) is the phenomenon of transmission and integration of genes between different organisms[16]. HGT is known to provide new

adaptability in microorganisms and allow colonization in new environments[17]. Recently, the installation of IBP through HGT was suggested for several sea-ice algae[18,19]. The evidence for this hypothesis include the (i) phylogenetic discrepancies of the species and genes, (ii) lack of IBP genes in closely-related species in warmer regions, and (iii) lack of intron in some of eukaryote-derived IBP genes. It is hence speculated that the cold adaptation of the microbes is also indebted to HGT. In addition, Raymond (2014)[20] reported that two putative IBPs from ascomycetes are less similar to those from basidiomycetes and suggested HGT in the ascomycetes. However, the primary-to-tertiary structures of ascomycete IBPs remain to be elucidated.

Antarctomyces psychrotrophicus is currently the sole ascomycete whose IBP (AnpIBP) production is confirmed[21]. Only a 20-residue peptide sequence was determined for the N-terminal region of AnpIBP, whereas the full sequence and homogeneity to known IBPs that contain the DUF3494 sequence remain unclear. Since *A. psychrotrophicus* is one of the dominant species isolated from several different substrates in Antarctica, such as soils[22], waters in lakes[23], and marine macroalgae[24], they are exposed to freeze-thaw cycles. IBP production may therefore be a key determinant of cold adaptation of *A. psychrotrophicus*. To clarify the evolutionary process and physiological role of ascomycete IBPs, we analyzed the cDNA and peptide sequences of AnpIBP and examined their phylogenetic relationship with other microbial IBPs. The model structure and ice-binding properties of AnpIBP were also examined and compared with other microbial IBPs. We discuss the cold-adaptation strategy of *A. psychrotrophicus* and the evolutionary relationship among microbial IBPs based on these results.

2.3. Materials and methods

2.3.1. Preparation of cDNA library, and total cDNA analysis of A. psychrotrophicus

A. psychrotrophicus strain Syw-1 was isolated from soil collected from Kizahashi-hama, Skarvsnes on the Soya coast, Antarctica, in 2006 and cultured in our laboratory in PDB medium. The cultures were kept at either −1°C or 15°C for 1 month to compare the efficiency of IBP expression between the two temperatures. Total RNA of *A. psychrotrophicus* was extracted and purified using the RNeasy Plant Mini Kit (QIAGEN, CA, USA), according to the suggested protocol. Poly (A+) RNA was isolated by oligo (dT) cellulose chromatography (New England Biolabs, MA, USA). cDNA was synthesized using the Marathon cDNA Amplification Kit (BD Biosciences Clontech, CA, USA). The constructed library was sequenced with the Illumina HiSeq™ 2000. The raw reads were cleaned by removing adaptor-only reads, repeated reads, and low-quality reads by Illumina Sequencing Analysis Pipeline ver. 1.6. Transcriptome de novo assembly was carried out with short reads assembling program Trinity[38]. IBP sequences were identified using BLAST (http://blast.ncbi.nlm.nih.gov/Blast.cgi).

To confirm the accuracy of the determined cDNA sequences and to obtain intron information, the AnpIBP1b gene was amplified from the genome of *A. psychrotrophicus* by PCR with forward primer 5′-ATGGTTTCCGCCTTCATGATCC-3′ and reverse primer 5′-TTAGACCTTGAAGAACTTGGCAGA-3′, which are the 5′- and 3′-terminal cDNA sequences of AnpIBP1b, respectively. AnpIBP2 gene was also amplified with a forward primer 5′-GCATCGTTCGCTGTTCTAGGAG-3′ and a reverse primer 5′-GGAGGTAGTAGTAGTGGTTGTGGT-3′. The genome of *A. psychrotrophicus* was purified, as described in [39]. The PCR reaction was performed with TaKaRa Ex Taq (TaKaRa, Shiga, Japan). The PCR product was cloned into a pMD20-T vector (Mighty TA Cloning Kit; TaKaRa, Shiga, Japan), transformed into *Escherichia coli* JM109, and then sequenced.

2.3.2 Sequence alignment and structural modeling of AnpIBP

Multiple sequence alignment was performed with the Clustal omega tool (http://www.ebi.ac.uk/Tools/msa/clustalo/) using default parameters. The same tool was used to examine the sequence identities.

The structural models of AnpIBP1a and AnpIBP2 were prepared with MODELLER (http://salilab.org/modeller/) and visualized with Chimera (http://www.cgl.ucsf.edu/chimera/). TisIBP8 (pdb code = 5B5H), LeIBP (3UYU), FfIBP (4NU2), ColIBP (3WP9), and IBPv_a (5UYT) were used as templates. A total of 10

models were created for each isoform, and an energy-minimized structure was selected on the basis of the MODELLER score (DOPE).

2.3.3. Phylogenetic analysis of microbial DUF3494 domains

The MEGA7 software (http://www.megasoftware.net/) was used to create the phylogenetic trees based on the microbial DUF3494s and 16/18S ribosomal RNA sequences. The former (DUF3494 tree) was made with maximum likelihood method based on the WAG+F+G model[40]. The bootstrap values were obtained with 500-resamplings. The latter tree (rRNA tree in Fig. 2.4B) was prepared by employing the neighbor-joining method based on the TN93+G model[41]. Only Bayesian inference tree was made by using Mrbayes software ver. 3.2.6 (http://www.mrbayes.sourceforge.net/download.php) with using 400,000 generations (four chains), sampling once every 100 rounds, random starting tree, WAG amino acid substitution model, and discarding a burn-in of 1,000. The AU test[42] and SH test[43] were performed with using Treefinder software (http://www.treefinder.de/).

2.3.4. Expression and purification of recombinant and native AnpIBPs

Codon-optimized AnpIBP1a gene (Ala^{1}–Val^{216}) with 5′-terminal *Xho*I and Kex2 signal cleavage sites (ctcgagaaaaaga) and 3′-terminal *Not*I (gcggccgc) sites was synthesized and digested with the restriction enzymes. The resultant DNA fragment was ligated into pPICZα (Thermo Fisher Scientific, MA, USA) digested with the two restriction enzymes. The expression vector containing the AnpIBP1a gene was linearized using the *Pme*I restriction enzyme. Transformation of the *P. pastoris* X33 strain was performed using the *Pichia* EasyComp Transformation Kit (Thermo Fisher Scientific, MA, USA). The transformant was selected by Zeocin resistance and the IBP expression level. The selected transformant was cultured in 80 mL of buffered glycerol complex medium (1% yeast extract, 2% peptone, 100 mM potassium phosphate at pH 6.0, 1.34% YNB, 4×10^{-5}% biotin, and 1% glycerol) at 28°C with agitation. When OD_{600} reached 10, the cells were harvested by centrifugation at 7500 rpm for 10 min at room temperature and were then resuspended in 450 mL of 2× buffered methanol complex medium (2% yeast extract, 4% peptone, 200 mM potassium phosphate at pH 6.0, 2.68% YNB, 8×10^{-5}% biotin, and 0.5% methanol). The cells were cultivated in a 1-L BMJ-01P fermenter (ABLE, Tokyo, Japan) at 20°C. Methanol was continuously added to the fermenter through a peristaltic pump at a manually controlled flow rate of 0.5–3.5 mL/h. After 96–120 h of cultivation, the medium containing IBP was collected by centrifugation and was dialyzed against 20 mM Gly-HCl buffer (pH 3.0). The

dialysate was loaded into a High-S (Bio-Rad, CA, USA) column and eluted using a 0–300-mM NaCl linear gradient over 10-column bed volumes. The antifreeze active fractions were recovered and dialyzed against 20 mM Tris-HCl (pH 8.0). The dialysate was applied into a High-Q (Bio-Rad, CA, USA) column and eluted using a 0–300-mM NaCl linear gradient over 10-column bed volumes. The recovered fraction was concentrated to a 5-mL volume and further purified by gel-filtration chromatography using Superdex 200 (GE-Healthcare, Amersham, UK) equilibrated with 20 mM Tris-HCl buffer containing 500 mM NaCl. The antifreeze active fractions were collected and dialyzed against water. The purity of the sample was checked using 16% SDS-PAGE stained with CBB.

All mutants were prepared using the KOD-plus Mutagenesis Kit (Toyobo, Osaka, Japan) and confirmed by DNA sequencing. Then, they were expressed and purified by the same procedure as that used for the wild types. In the case of His-tagged mutants, the first purification on the High-S column was substituted with the Ni-NTA column (QIAGEN, CA, USA) equilibrated with 20 mM Tris-HCl (pH 8.0) containing 500 mM NaCl. His-tagged AnpIBPs were eluted with the same buffer containing 250 mM imidazole.

Native AnpIBP was purified from the culture supernatant of *A. psychrotrophicus*, as described elsewhere[21].

2.3.5. Measurement of TH activity and IRI

The TH activity was measured with a photomicroscope system equipped with a temperature-controlling system, as described in[44], with slight modifications. Briefly, IBP was dissolved in 20 mM Tris-HCl (pH 8.0). The sample solution (1 μL) in a glass capillary was placed on the stage and cooled rapidly to approximately −25°C until frozen. The frozen sample was melted slowly until a single ice crystal remained. The temperature at which the ice crystals melted was recorded as *Tm*. The formed ice-crystal was kept at *Tm* − 0.1°C for 5 min. The temperature was slowly lowered (0.1°C/min). The freezing point (T_f) of the sample was determined as the temperature at which rapid ice growth was observed. The TH values were evaluated from the absolute value of the difference between T_m and T_f (i.e., TH = $|T_f - T_m|$).

IRI of IBPs was measured by the observation of the change in the ice crystal morphology under the photomicroscope. Recombinant AnpIBP1 dissolved in 30% sucrose solution (1.2 μL) was sandwiched between two glass plates. The sample was cooled at 55°C/min until the entire solution was frozen. Then, it was warmed at 20°C/min up to −3°C and incubated for 1 h. A snapshot was taken every 15 min. The

size of the ice crystals was measured using ImageJ software (http://imagej.nih.gov/ij/).

2.3.6. Observation of ice crystal morphology in the AnpIBP solution

The *A. psychrotrophicus* culture (3 μL) cultivated at 4°C or pure PDB medium was placed on a glass plate and observed under a photomicroscope equipped with a temperature controller. The sample solution was frozen entirely by decreasing the temperature to approximately −25°C, which created a tight assembly of numerous single ice crystals. These crystals were then melted by increasing the temperature to −1°C in order to decrease the number of ice crystals formed. The ice crystals were then allowed to grow by decreasing the temperature at the rate of 1°C/min, and their morphologies were observed.

To observe the macroscale ice texture, 25 mL of *A. psychrotrophicus* culture or pure PDB medium in a 50-mL tube was frozen at −20°C for 24 h.

2.3.7. Freezing–thawing cycle experiments of A. psychrotrophicus

The mycelia of *A. psychrotrophicus* and *T. ishikariensis* were cultured in 50 mL of PDB medium at 10°C. After growth of the mycelia, the cultures were transferred to an incubator at −1°C to induce IBP expression. After 1 month, the cultures were made to undergo 25 cycles of freezing at −20°C and thawing at room temperature. The cells were grown on a PDA plate at 10°C, and the growth rates of the mycelia were recorded.

2.4 Results

2.4.1. Three AnpIBP isoforms were identified from total cDNA analysis

Total cDNA analyses of *A. psychrotrophicus* cultivated at cold (−1°C) and moderate (15°C) temperatures were performed to obtain the complete sequences of AnpIBP. We obtained a total of 27,265,280 clean reads (-1°C) and 27,764,816 clean reads (15°C) that are 94.21% and 94.09% of the raw reads, respectively. The de novo assembly identified a total of 16,659 unigenes of 1,162-nt average length for −1°C and a total of 13,831 unigenes of 1,249-nt average length for 15°C. Blast search identified three candidate sequences of AnpIBP from the unigenes. These sequences matched a lot of microbial IBP sequences, such as that of *Chloromonas brevispina* IBP, indicating that AnpIBPs are homologous to other microbial IBPs that contain the DUF3494 sequence. Two of the three cDNA sequences were identified only in the cells cultivated at −1°C, suggesting that their expression occurs only at low temperatures. Fig. 2.1A shows the previously identified 20-residue amino acid sequence[21] (native AnpIBP) and three newly translated amino acid sequences, designated as AnpIBP1a (236 residues), AnpIBP1b (245 residues), and AnpIBP2 (242 residues, identified as a partial sequence). The former two isoforms are perfectly identical except for their C-terminal regions (after the 203th residue), which were not observed in other microbial IBPs. In contrast, the former two isoforms (AnpIBP1a and 1b) and the latter (AnpIBP2) exhibited only 44% sequence identity. The C-terminal region of AnpIBP1a mainly comprises hydrophobic and positively charged residues, whereas that of AnpIBP1b contains one positive, two negative, and several hydrophobic residues. In both AnpIBP1a and 1b, the Ala1−Ala20 sequence almost matches the known 20-residue sequence of native AnpIBP secreted toward the extracellular space. Therefore, the 19-residue N-terminal sequence before Ala1 (Met18−Ala0: MVSAFMILCVLGSAFVSNA) was assigned to the signal peptide. The molecular weights (M.w.) excluding the signal peptide were hence estimated to be 21.4 and 23.0 kDa for AnpIBP1a and 1b, respectively. They are, however, not consistent with the SDS-PAGE result for purified native AnpIBP, indicating that it is 24 kDa (see below). This discrepancy can be attributed to the post-translational modification of the native protein, where Asn55 in the glycosylation sequence Asn-X-Ser/Thr (X is any amino acid residue, except proline) is presumably modified with N-linked glycan.

To obtain information on introns, the genes of AnpIBP1b and AnpIBP2 were amplified from the *A. psychrotrophicus* genome by PCR with primers based on the cDNA sequences. The AnpIBP2 gene amplified from the genome were consistent with

the cDNA sequence, indicating the existence of a gene in the genome without an intron. In contrast, the AnpIBP1b gene has two introns (Fig. 2.1B). Introns 1 and 2 were found to be of length 49 and 63 bp, respectively, and both followed the "GT-AG splicing rule." Intron 1 was located near the boundary between the signal peptide and mature IBP domain. In contrast, intron 2, located at the end of the IBP domain, contained the C-terminal sequence of AnpIBP1a, including the terminator codon. When intron 2 was spliced, the mRNA product matched perfectly with the cDNA sequence of AnpIBP1b. This finding indicates that intron 2 can be cleaved by an ambiguous splicing signal for the creation of two types of mRNA (AnpIBP1a and 1b) from one AnpIBP gene (Fig. 2.1C).

2.4.2. The beta-helical structure was modeled for AnpIBP

Based on the primary sequence information, the model structures of AnpIBP1a and AnpIBP2 were constructed using the MODELLER software with five microbial IBP structures (i.e., TisIBP8, LeIBP, FfIBP, ColIBP, and IBPv_a) as templates. The principle constituent of AnpIBP1a was apparently a seven-ladder β-helix with a triangular cross-section with an accompanying α-helix alongside (Fig. 2.2A), which is similar to the construction in other microbial IBPs[14]. The inward-pointing residues in the model constructed a hydrophobic core, which is generally indispensable for the stabilization of the β-helix. The three flat surfaces are called the A, B, and C faces. Among them, the B face is suggested to be an ice-binding site (IBS) in the known microbial IBP structure. This putative IBS comprises no regularly arrayed residues (Fig. 2.2B), different to the hyperactive IBPs identified from insects[25]. Significantly, most of the outward-pointing residues on the putative IBS were glycine, alanine, serine, and threonine, which contain a relatively small side-chain group. The "anchored clathrate water hypothesis[26]" predicts that the combination of hydroxyl (hydrophilic) and methyl (hydrophobic) groups tends to form a water network on IBS, which anchors the host protein to the ice crystal surfaces.

Although the overall structures of AnpIBP1a and AnpIBP2 were mostly identical (Cα RMSD = 0.482 Å), the amino acid compositions of their IBSs were different (Fig. 2.2B). The IBS of AnpIBP2 is more hydrophilic as it locates more Ser and Thr, but it has fewer Ala compared with AnpIBP1, suggesting that AnpIBP1 and AnpIBP2 possess different ice-binding properties.

In the model structure of AnpIBP1a, the N-glycosylation site (Asn55) is located at the N-terminal end of the long α-helix, which seems distant from the putative IBS. This assumption is supported by the fact that the removal of glycan did not affect

the ice-binding property (see below). N-glycosylation may function for protein folding and stability rather than for ice binding, as has been suggested for known IBPs[27]. For both AnpIBP1a and 2, our modeling approach could not predict the structure of the C-terminal segment following the DUF3494 sequence because this region has no structural template.

2.4.3. IBPs from ascomycetes and basidiomycetes have evolved independently

Protein Blast searches using the full amino acid sequences of AnpIBP1 and 2 showed that the related sequences were mostly DUF3494-containing proteins from ascomycetes or bacteria. Most of the latter were found to be actinobacteria, such as *Streptomyces*, *Arthrobactor*, and *Kitasatospora* species. The peptide sequence exhibiting the highest identity and similarity to AnpIBP1 was a putative IBP from an ascomycete *Zymoseptoria tritici* (58% and 66%) and that to AnpIBP2 was a putative IBP from a planctomycete *Paludisphaera borealis* (72% and 76%). Such high identities were also observed at the nucleotide level; identity of mRNA between AnpIBP1 and the putative IBP from *Z. tritici* was 59%, and that between AnpIBP2 and *P. borealis* was 61%. The mRNA-based identity was slightly lower for *P. borealis*, which might be due to a difference of codon usages (3rd codons); GC content of AnpIBP2 was 50%, while that of the IBP from *P. borealis* was 65%. In contrast, both AnpIBP1 and AnpIBP2 exhibited low sequence identity with basidiomycete-derived IBPs, such as TisIBP8 from *Typhula ishikariensis* and LeIBP from *Leucosporidium* sp. AY30 (29%–36%), although ascomycetes and basidiomycetes are phylogenetically close.

Another difference between ascomycete and basidiomycete IBPs was found at a specific portion of their sequences, which creates a capping structure at the end of their β-helical domains (Fig. 2.3). As can be seen in this figure, this portion exhibits a significant variation in the structures of microbial IBPs, and its construction in the AnpIBP model showed a significant similarity with that of *Flavobacteriaceae* bacterium isolate 3519-10 (IBPv_a). Do *et al*. (2014) proposed that microbial IBPs can be divided into two groups based on their capping structure[28]. Our sequence alignments, however, suggest that microbial IBPs can be divided into three groups. Group 1 and group 2 have large capping structures where a disulfide-bond is only contained in the latter, which is identical to the classification by Do *et al*. Our alignment further suggests the existence of group 3 that includes ascomycete AnpIBP, bacterial EfcIBP, StaIBP (putative IBP), and IBPv, all of which have a small capping structure. Similarity of DUF3494 sequences within each group are high, while those between the groups are low (Table 2.1). When all fungal putative IBP sequences in the database (~200) containing the

capping loops were aligned, it was found that ascomycete- and basidiomycete-derived putative IBPs have small and large capping structure, respectively. In contrast, the capping structures of bacterial putative IBPs are variable depending on the species.

To investigate the evolutionary history of ascomycete IBPs, we created and compared the phylogenetic trees of the microbes based on their DUF3494-peptide sequence (DUF3494 tree, Fig. 2.4A) and on their 16S/18S ribosomal RNA genes (rRNA tree, Fig. 2.4B). Comparison between these two trees is commonly used to identify the phylogeny of IBPs[19,29]. In Fig. 2.4B, ascomycetes, basidiomycetes, bacteria, and algae were separately categorized, and the former two shared a common node, which is consistent with the universal tree of their life. Significantly, the DUF3494 tree created by maximum likelihood (ML) method (Fig. 2.4A) showed that microbial DUF3494s are separated into three groups similarly to that in Fig. 2.3A. The sequences in group 1, 2, and 3 have large, disulfide-bonded, and small capping structures, respectively. Note that in Fig. 2.4A, group 3 was sub-divided into Groups 3a and 3b, as several bacterial sequences including IBPv are different from the other bacteria, although they have small capping structures. Thus, ascomycetes formed a different clade from basidiomycetes but shared a common node with several bacteria, which is inconsistent with the ribosomal RNA tree. The DUF3494 tree (Fig. 2.4A) shows that AnpIBP1 and 2 (*Antarctomyces psychrotropicus* isoform 1 and 2) belong to different clades within Group 3A, and the latter shares a common node with a bacterium *P. borealis*. Such phylogenetic incongruence is generally explained by HGT. Note that almost the same phylogenetic relationships were observed in the Bayesian inference (BI) tree of DUF3494 sequences, whose bootstrap values were shown in Fig. 2.4A.

The DUF3494 phylogenetic tree is highly similar to that presented by Bayer-Giraldi, M. et al. (2010)[18] and also consistent with the other reports dealing with HGT of IBPs. For example, algal *Chloromonas brevispina* and *Chlamydomonas raudensis* IBPs are distant from the other algal IBPs but close to bacterial and/or ascomycete ones in the phylogenetic tree, which agrees with the previous reports hypothesizing probable acquisition of these IBPs by HGT[20,30]. Other examples are IBPs from bacterial symbiont of *Euplotes focardii,* which were separated into group 3a and 3b and shared a common node with *S. aurantiaca* or *Flavobacteriaceae* bacterium isolate 3519-10 in the phylogenetic tree. This also agree with the report presenting that EfcIBPs are possibly derived from close relatives of these species[31].

To confirm the difference of the tree-topologies between Figs. 2.4A and 4B is not ascribed to tree-reconstruction artefact, statistical tests denoted “approximately unbiased (AU) test” and “Shimodaira-Hasegawa (SH) test” were performed. The upper

trees in the red box of Fig. 2.5 shows the ML and BI trees of the DUF3494-peptide sequences from bacteria, ascomycetes, and basidiomycetes in group 2 and 3A. Again, topologies of the ML and BI trees are almost identical, and ascomycetes (reds) are phylogenetically close to bacteria (yellows) rather than basidiomycetes (greens). We then created the trees with a topological constraint (denoted Constrained tree 1) that intentionally separates ascomycetes, basidiomycetes, and bacteria into different clades (i.e., null hypothesis). The ML and BI tree topologies were evaluated against the null hypotheses by using the statistical tests. The question here is that the null hypotheses are significantly worse ($p<0.05$) than the non-constrained topologies or not. The AU and SH tests evaluated small p-values (0.006–0.018) for the null hypotheses (Test1 table, in Fig. 2.5), suggesting a significant phylogenetic incongruence exists between the host species and DUF3494 sequences.

Additional statistical test was performed to confirm whether the AnpIBP isoforms belong to different clades or not. In this case, the evaluation was performed with using Constrained trees 2 (Fig. 2.5, blue boxes), where AnpIBP1 and 2 are monophyly and that they were placed next to each other. The AU and SH tests evaluated small values (0.000–0.002) for these trees (Fig. 2.5, Test2 table), suggesting the independency of the evolutionary processes of these two AnpIBP isoforms.

2.4.4. AnpIBP1 is moderately active but creates a lemon-like ice crystal

The recombinant protein of AnpIBP1a was synthesized by employing the *Pichia pastoris* expression system and purified with the combined use of ion-exchange and gel-filtration chromatographies. The M.w. of purified recombinant AnpIBP1a was estimated to be 25 kDa by SDS-PAGE (Fig. 2.6A), inclusive of a 216-residue peptide (of approximately 21.4 kDa in size) and an N-linked glycan bound possibly to the Asn55 glycosylation site. A smeared band observed between the 25- and 35-kDa regions in SDS-PAGE may be due to multiple components of the glycan because *P. pastoris*-derived proteins generally do not migrate to this position. A slightly lower M.w. of native AnpIBP (24 kDa) suggests a difference in the compositions of the N-glycan attached to the two proteins.

Recombinant AnpIBP1a at a concentration of 150 μM was capable of stopping the growth of a single ice crystal and had a TH activity of 0.56°C (Fig. 2.6B, black). This value is identical to that of a purified native AnpIBP sample at the same concentration (Fig. 2.6B, green), which confirms the accuracy of the determined AnpIBP sequences. It has been well demonstrated that “moderately active IBP” shapes an ice crystal into a bipyramidal morphology and exhibits approximately 1°C of the TH

activity at millimolar concentrations[32]. In contrast, a lemon-like ice crystal and approximately a 2°C–4°C temperature of high TH values is obtained for "hyperactive IBPs" at micromolar concentrations. Therefore, recombinant AnpIBP1a should be categorized into moderately active IBPs based on its TH value (0.7°C at 300 μM), although this protein simultaneously showed its ability to create lemon-like ice crystals (Fig. 2.6C) like a hyperactive IBP. This lemon-like ice crystal in the AnpIBP1a solution underwent a bursting growth along the *c*-axis to form a large hexagonal bipyramid (Fig. 2.6D) when the temperature fell below the depressed freezing point. These results are indicative of a unique ice-binding manner of AnpIBP1a.

AnpIBP1a contains an N-glycan possibly at Asn55 and an extra C-terminal segment after the 203th residue, which are not conserved in the other microbial IBPs. Hence, they may contribute to the ice-binding property of this protein. To examine such a possibility, a non-glycosylated mutant (AnpIBP1a_N55D) and a mutant containing no C-terminal segment (AnpIBP1_N55D) were recombinantly expressed by *P. pastoris* similarly to the wild type, and their TH activities were assessed. The substitution of Asn55 with Asp decreased M.w. from 25 to 21 kDa on SDS-PAGE (Fig. 2.6A), indicating the presence of an N-glycan at Asn55. The TH and ice-shaping activities of the two mutants were almost identical to those of the wild type (Fig. 2.6B). The His-tagged versions of these two mutants also demonstrated the same TH values as those without the tag. These results indicate that neither an N-glycan nor the C-terminal segment is involved in ice binding. The average yields of recombinant AnpIBP1 per culture were found to be approximately 10, 110, 90, 160, and 170 mg/L for AnpIBP1a, AnpIBP1a_N55D, AnpIBP1_N55D, His-AnpIBP1a_N55D, and His-AnpIBP1_N55D, respectively.

2.4.5. AnpIBP1 strongly inhibits IR

IR is a phenomenon of the increase in the ice crystal size within already frozen materials. One of the principle abilities of IBP is the inhibition of recrystallization through binding onto the ice crystal surfaces[6,7]. To evaluate this ability of IBP, termed IR inhibition (IRI), for recombinant AnpIBP1a wild type, we monitored the growth of ice crystals in a frozen AnpIBP1a solution supplemented with 30% sucrose after annealing for 60 min at subzero temperature (−3°C). In the absence of AnpIBP1a, an apparent growth of ice crystals was observed after 60 min of annealing, and the average size of the crystals was recorded to be approximately 393 μm^2 (Fig. 2.7). The ice crystal growth was significantly arrested with the addition of only a small amount of AnpIBP1a (5 μM), where the average ice crystal size was approximately 8 μm^2, indicating that this

protein possesses strong IRI activity. On dilution to 0.5 μM, AnpIBP1a allowed crystal growth up to a size of 164 μm^2, but a further dilution to 0.05 μM almost failed to stop the growth (333 μm^2). These results are in good agreement with previous indications that native AnpIBP possesses IRI ability at approximately a 2-μM concentration[21].

2.4.6. Native AnpIBP affects the growth of ice crystals even at a very low concentration

We observed a trend of freezing of a potato dextrose broth (PDB) medium in the absence/presence of AnpIBP, for which a 3-μL droplet of each sample was frozen on the stage of a photomicroscope. For the pure PDB medium without AnpIBP, relatively large ice crystals with a rounded, leaf-like shape were observed (Fig. 2.8A; right). This is the typical observation for a solution without IBP. In contrast, numerous rock-like, fine ice crystals were generated in *A. psychrotrophicus*-containing medium cultivated at 4°C for 1 month, thereby including AnpIBP (Fig. 2.8A; left). On a macroscale, the culture supernatant of *A. psychrotrophicus* turned white and opaque (Fig. 2.8B) when frozen at −20°C, indicating the formation of numerous fine ice crystals. When this culture medium was loaded onto SDS-PAGE, no significant band was detected by Coomassie brilliant blue (CBB) staining. These results again suggest that AnpIBP can create a fine ice texture at the micromolar level.

To assess the physiological functions of AnpIBP, we compared the growth of the mycelia of *A. psychrotrophicus* on potato dextrose agar (PDA) plates before and after 25 cycles of freeze and thawing. A snow mold fungus *T. ishikariensis* was also tested for comparison. These cell cultures were maintained at −1°C to induce IBP expression before starting the cycles. It was found that both fungi grew at 10°C without the cycles (Fig. 2.8C), where the growth rates were 0.5 cm/day for *A. psychrotrophicus* and 0.1 cm/day for *T. ishikariensis*. Significantly, *A. psychrotrophicus* grew normally on the plate even after the 25 freeze-thaw cycles, while *T. ishikariensis* did not show any growth, indicating that *A. psychrotrophicus* is extremely tolerate to freeze-thaw cycles.

2.5 Discussion

In cold environments, many psychrophilic microbes, including fungi, produce IBPs to control ice crystal growth, which has detrimental effects on their tissues. The fungi are categorized into two major phyla, Ascomycota and Basidiomycota. A sole ascomycete IBP from *A. psychrotrophicus* (AnpIBP) was initially characterized in our previous report. Here, we determined the cDNA and peptide sequences of three AnpIBP isoforms to examine their structures and ice-binding properties, which revealed the uniqueness of their phylogenetic background and functional abilities.

2.5.1. cDNA and peptide sequences reveal the structure of AnpIBP

Most of the microbial IBPs are known to contain the DUF3494 sequence, whereas the DUF3494-containing proteins detected in the ascomycete genomes or cDNA libraries have not been confirmed to exhibit the ice-binding property. The ascomycete DUF3494-proteins share a high homogeneity with the three AnpIBP isoforms, and some of them can be assigned to the microbial IBPs. For example, Kawahara *et al*.[33] reported that several Antarctic ascomycetes produce extracellular substances that modify the ice crystal shape, some of which could be IBPs.

The N-terminal sequences of AnpIBP1a and AnpIBP1b almost completely matched with the previously determined sequence of native AnpIBP (Fig. 2.1A), suggesting the secretions of both AnpIBP isoforms toward the extracellular space via the signal peptide. This finding is consistent with the present finding showing that recombinant AnpIBP1a possesses almost the same TH activity as that of the native AnpIBP (Fig. 2.6B). In contrast, AnpIBP2 was not found in the culture supernatant of *A. psychrotrophicus*. Thus, this isoform may exist in the intracellular space or on the cell surface. Recently, several reports have shown the existence of such non-secreted IBPs[34,35].

Our intron analysis revealed that AnpIBP1a and 1b are produced from one IBP-coding region through alternative splicing of the C-terminal non-ice-binding region (Fig. 2.1C). The existence of two isoforms that differ only at the C-terminal segment evoked a question about its relevance to the structure and function of this protein. However, the removal of the segment did not affect the ice-binding property of AnpIBP1a (Fig. 2.6B). The extension of the N- or C-terminal sequence has sometimes been observed in several IBPs, suggesting that these regions are mostly variable and not conserved. Although their functions have hardly been clarified, several reports have suggested that such additional sequences are responsible for dimerization[14] or anchoring of the protein to the cell surface[35,36]. The additional C-terminal sequences of AnpIBP1a

and 1b have electrically opposite features (Fig. 2.1A). Thus, these segments may be involved in heterodimerization or binding to different substrates other than ice.

2.5.2. AnpIBP isoforms may originate from different bacteria

The comparison of the AnpIBP sequences with that of other microbial IBPs revealed that AnpIBP1 and AnpIBP2 share high sequence identities with the DUF3434-containing proteins of both ascomycetes and bacteria (<72%) but poor identities with those of basidiomycetes (<36%). In the phylogenetic tree of DUF3494 domains (Fig. 2.4A), ascomycete DUF3494s, including AnpIBPs, were phylogenetically far from the basidiomycete ones but close to the bacterial ones in group 3, which is inconsistent with the phylogenetic relationship of their life (Fig. 2.4B). This phylogenetic incongruence suggests that ascomycete IBPs independently evolved from basidiomycete IBPs and that they were possibly acquired from bacteria through HGT. The statistical tests (Fig. 2.5, Test 1) further support this HGT hypothesis. These results are in good agreement with the proposition by Raymond[20] and support the structural similarity in the capping loop region of DUF3494 proteins (Fig. 2.3). All of the DUF3494 proteins in group 3 contain a small capping structure, whereas those from other groups have a different capping structure. This semi-conserved region may have a significant correlation with the evolutionary process of microbial DUF3494. Another evidence of the HGT hypothesis is the occurrence of differences in the number of introns. AnpIBP1 and 2 genes do not possess any introns in the DUF3494 sequence (Fig. 2.1B and C), which may be due to the occurrence of HGT from bacteria. It has been reported that basidiomycete IBPs from yeast[11] and mushrooms[12] have eight and four introns, respectively. Such a difference between IBPs from ascomycetes and basidiomycetes implies a difference in their evolutionary history and a relatively recent acquisition of ascomycete-derived IBP genes compared with those of basidiomycetes.

Such phylogenetic incongruence might also be explained by a different gene loss, in which DUF3494 genes were duplicated in an ancestor of fungi and bacteria, and they were lost differently during evolutionary process. If this is correct, some of the fungi should retain two or more kinds of DUF3494 that belong to different groups. All ascomycetes and basidiomycetes, however, possess only group 3 and group 1 DUF3494s, respectively. Furthermore, the DUF3494 gene has not been found in the other phyla of fungi, such as *Zygomycota* and *Chytridiomycota*. Since it is not likely that the DUF3494 genes were lost in all fungi other than ascomycetes and basidiomycetes, fungal IBP genes were possibly acquired by HGT.

The DUF3494 sequences of ascomycetes and bacteria in group 3 are scattered

in the phylogenetic tree (Fig. 2.4A). Furthermore, several DUF3494s from bacteria such as proteobacteria and flavobacteria are separated into the different groups. These results suggest that HGT of IBP occurs frequently.

Surprisingly, AnpIBP1 and AnpIBP2 in group 3 are apparently separated into different nodes. This finding is supported by the low sequence identity between AnpIBP1 and AnpIBP2 (44%), which is much lower than that between AnpIBP1 and ascomycete IBPs, such as *Z. tritici* IBP (58%), or that between AnpIBP2 and bacterial IBP, such as *P. borealis* IBP (72%). This significantly high sequence identity between AnpIBP2 and *P. borealis*-putative IBP indicates the installation of the IBP gene from this bacterium or its ancestor; thus, AnpIBP1 and AnpIBP2 presumably originate from different HGT events. This hypothesis was supported by another statistical test, which also negates monophyly of AnpIBP1 and 2 (Fig. 2.5, test 2).

In general, HGT hardly occurs between fungi (eukaryote) and bacteria (prokaryote) because of the difference in codon usage and incompatibility of promoters.[17]. However, it is known that HGT frequently occurs under specific stress from harsh environmental conditions and provides a selective advantage to the recipient organism[37]. Thus, extremely cold environments accompanied by ice crystal formation are likely to exert a strong selection pressure on microorganisms, and there is a strong demand for IBPs to adapt to this special environment. As a result of positive selection, several HGT events could occur and IBP-producing microorganisms could survive.

Most of the IBPs in group 3 were derived from ascomycetes or actinobacteria, both of which usually live in the soil, suggesting that the installation of the IBP gene through HGT progresses under cold soil environments. These microbes tend to form a community with the surrounding heterotrophic bacteria. In this dense community, physical contact between fungi and bacteria or among bacteria occurs frequently, thereby increasing the probability of HGT via a conjugation-like mechanism. Otherwise, the filamentous microbes may have acquired freely available IBP genes produced by lysis of neighboring microorganisms in the community. Another possibility is natural transformation due to cell membrane damage with high salt concentrations caused by ice crystal growth, which facilitate the incorporation of IBP genes into the cells. Kiko (2010)[13] proposed that sea-ice habitats create natural transformation conditions, enabling HGT. A similar scenario may be true in Antarctic soil because the continent is mostly covered with a large amount of snow and ice blocks.

2.5.3. AnpIBP facilitate the cold adaptation of A. psychrotrophicus

Because *A. psychrotrophicus* is isolated from various environments of

Antarctica[22-24], AnpIBP could play an important role in its cold adaptation. Our results suggest that AnpIBP1 is secreted into the extracellular space and is believed to be responsible for controlling ice growth around the cells. Nevertheless, the TH activity of AnpIBP1 (0.7°C at 300 μM) was not significant, although the environmental temperature is extremely low. For example, the minimum temperature at King George Island, where *A. psychrotrophicus* was first isolated, is −19.9°C[22]. AnpIBP1 showed both IRI (Fig. 2.7) and ice-shaping activities (Fig. 2.8A and B), even at extremely low concentrations (5 μM). Thus, the main function of this IBP will be the formation of fine ice crystals during freezing and the inhibition of IR during melting rather than freezing-point depression, which may lead to the prevention of freezing damages to the host organism. Indeed, *A. psychrotrophicus* can tolerate 25 freeze–thaw cycles, whereas the snow mold *T. ishikariensis* cannot (Fig. 2.8C). HGT between ascomycetes and bacteria may have significant importance for their cold adaptation and evolution, leading to the wide distribution of *A. psychrotrophicus* in Antarctica.

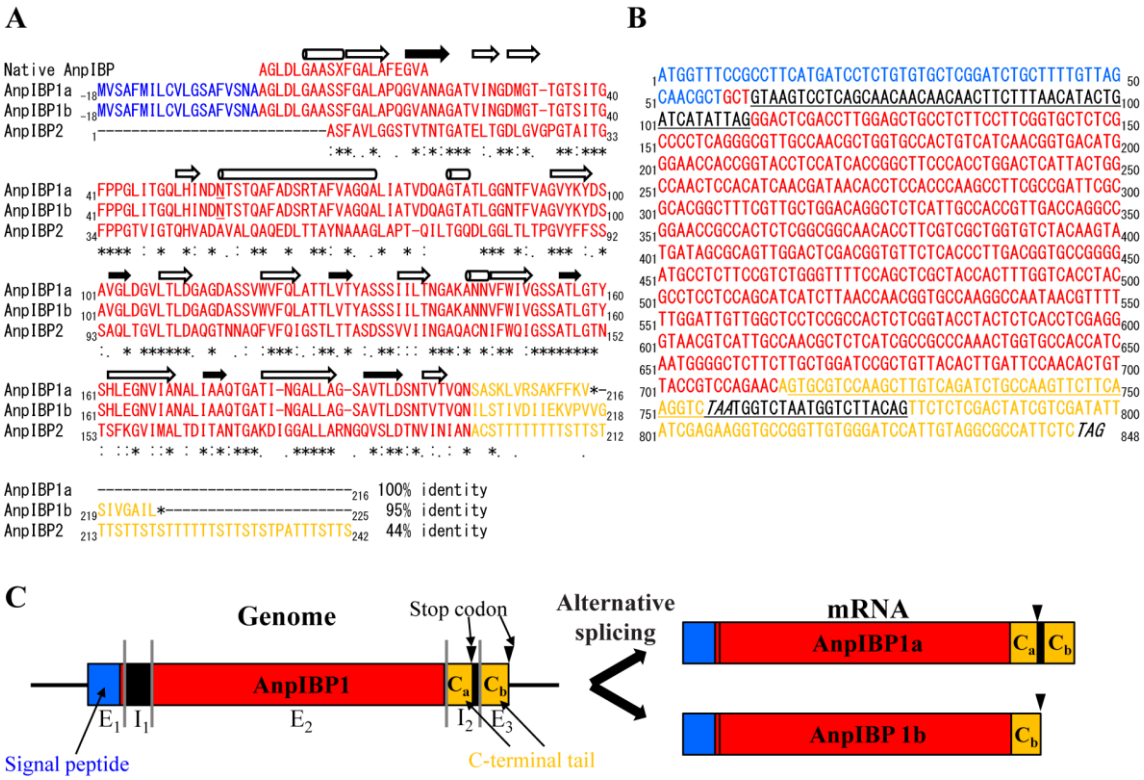

Figure 2.1. Sequence alignment of AnpIBP isoforms and genome structure of the AnpIBP1 gene. (A) The sequence alignment of translated amino acid sequences of AnpIBP isoforms identified by total cDNA analysis. Putative N-glycosylation (Asn55) sites of AnpIBP1 are underlined. Cylinders and arrows indicate alpha-helices and beta-sheets of the AnpIBP1 model, respectively. Black arrows particularly indicate beta-sheets that comprise the putative IBS of AnpIBP1. (B) Full-length AnpIBP1 gene in the genome. Introns are underlined. Terminator codons are shown in italic. (C) Schematic diagram of the genome structure and mature mRNA of AnpIBP. Ca and Cb indicate the C-terminal segment of AnpIBP1a and AnpIBP1b, respectively. Dotted lines indicate the splice positions. The AnpIBP1 gene in the genome comprises two introns (I) and three exons (E). The two types of mRNA are produced by alternative splicing of Exon 2. In all the figures, the signal peptide, untranslated region, DUF3494 region, and C-terminal segment are colored by blue, black, red, and yellow, respectively.

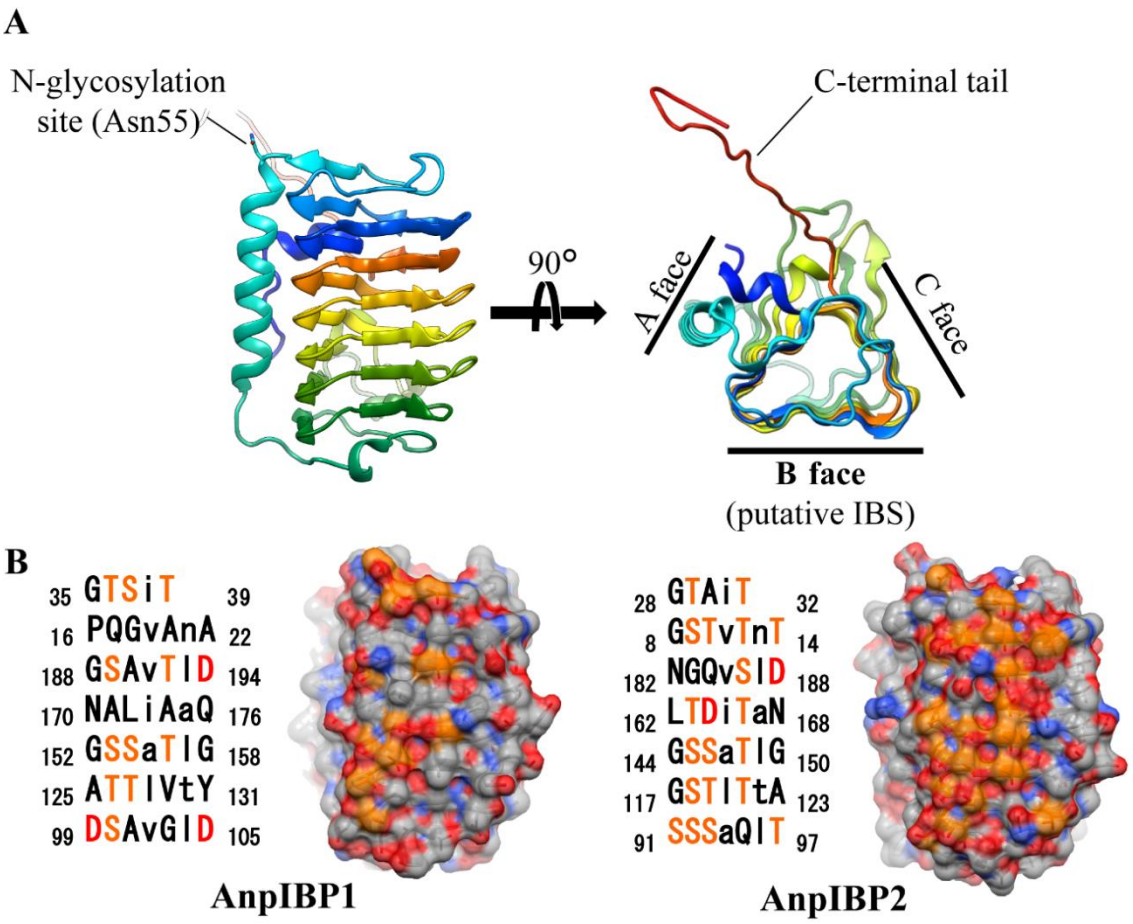

Figure 2.2. Structural model of AnpIBP. (A) The overall structure of AnpIBP1a is represented with a ribbon model in spectral color gradation from blue (N-terminus) to red (C-terminus). (B) Amino acid residues of the putative ice-binding sites (B face) of AnpIBP1a and AnpIBP2. Large and small letters indicate the outward- and inward-pointing residues, respectively. Serine and threonine residues are indicated in orange and positively charged residues in red.

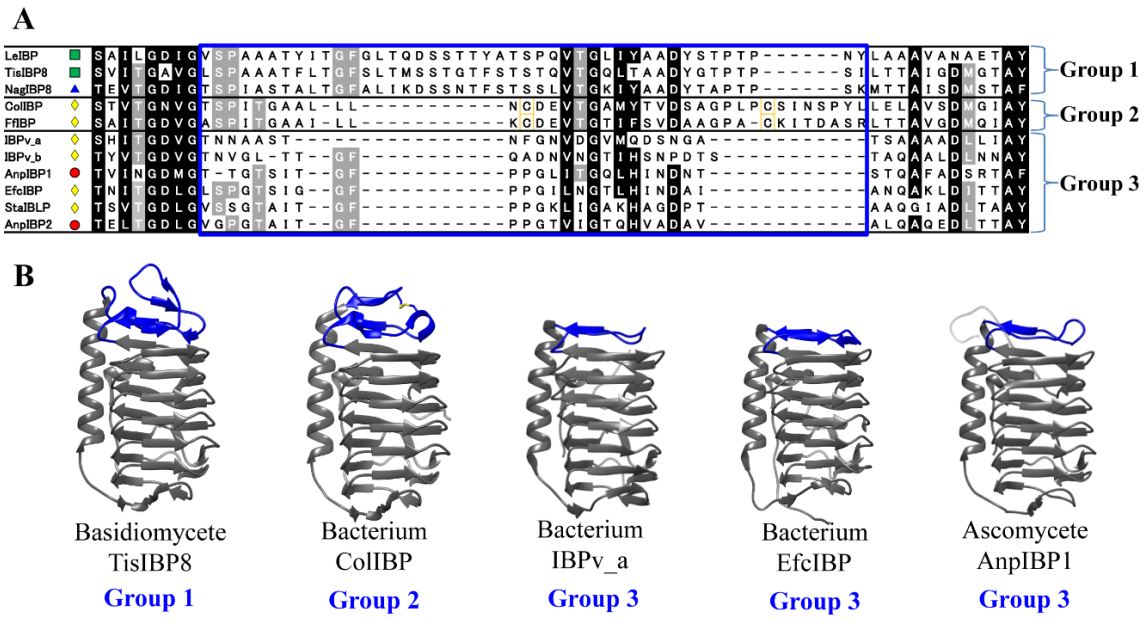

Figure 2.3. Sequence alignment of the capping structure between microbial IBPs. (A) Multiple sequence alignment among IBPs from *A. psychrotrophicus* (AnpIBP1, 2), bacterial symbiont of *Euplotes focardii* (EfcIBP), *Leucosporidium* sp. AY30 (LeIBP), *S. aurantiaca* (StaIBP), *T. ishikariensis* (TisIBP8), *Colwellia* sp. SLW05 (ColIBP), *Flavobacterium frigoris* (FfIBP), *Navicula glaciei* (NagIBP8), and *Flavobacteriaceae* isolate 3519-10 (IBPv). Sequences corresponding to the capping structure are in blue box. Cysteine residues involved in the disulfide bond are boxed with yellow. (B) Microbial IBP structures from each group. The crystal structures of ColIBP (pdb code: 3WP9), TisIBP8 (5B5H), IBPv_a (5UYT), and EfcIBP (6EIO) and the structural model of AnpIBP1a are shown as ribbon models, in which the capping structures are colored in blue.

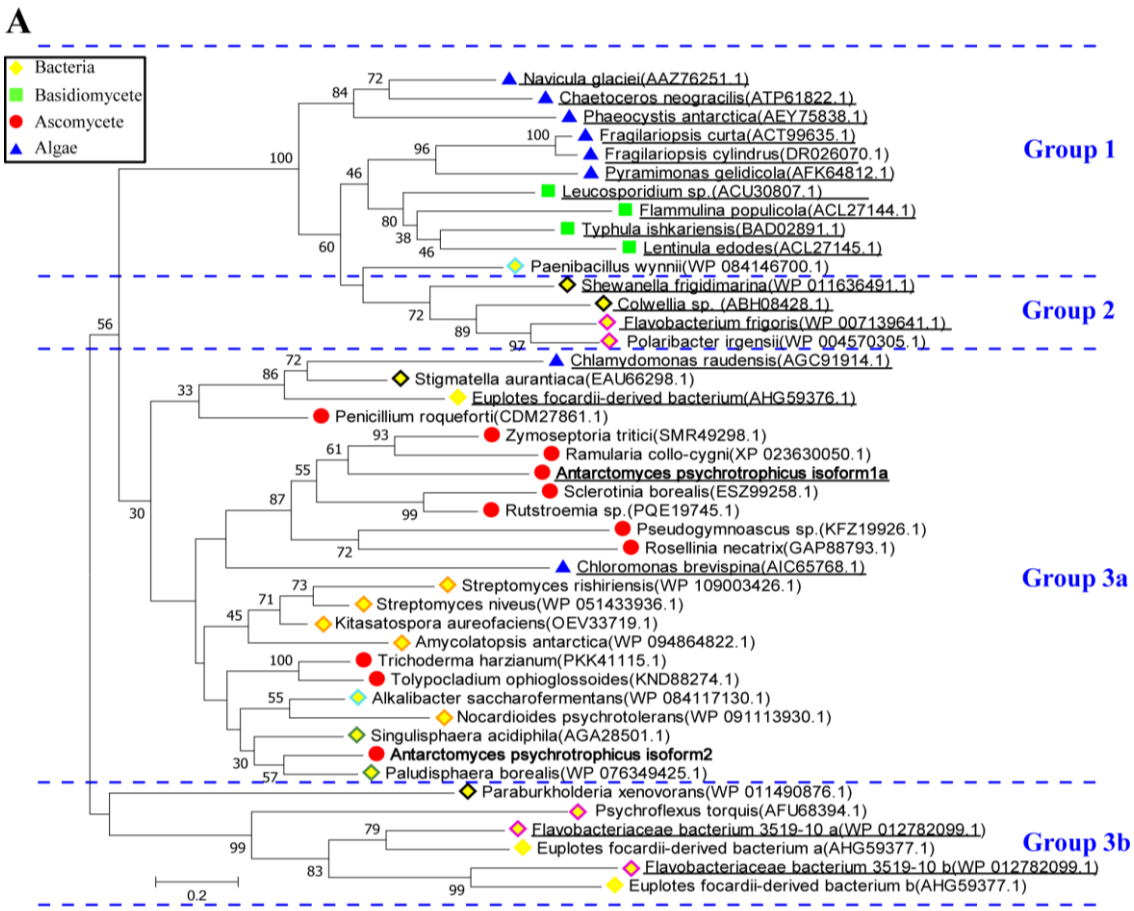
A
Bacteria
Basidiomycete
Ascomycete
Algae
Navicula glaciei(AAZ76251.1)
Chaetoceros neogracilis(ATP61822.1)
Phaeocystis antarctica(AEY75838.1)
Fragilariopsis curta(ACT99635.1)
Fragilariopsis cylindrus(DR026070.1)
Pyramimonas gelidicola(AFK64812.1)
Leucosporidium sp.(ACU30807.1)
Flammulina populicola(ACL27144.1)
Typhula ishkariensis(BAD02891.1)
Lentinula edodes(ACL27145.1)
Paenibacillus wynnii(WP 084146700.1)
Shewanella frigidimarina(WP 011636491.1)
Colwellia sp. (ABH08428.1)
Flavobacterium frigoris(WP 007139641.1)
Polaribacter irgensii(WP 004570305.1)
Chlamydomonas raudensis(AGC91914.1)
Stigmatella aurantiaca(EAU66298.1)
Euplotes focardii-derived bacterium(AHG59376.1)
Penicillium roqueforti(CDM27861.1)
Zymoseptoria tritici(SMR49298.1)
Ramularia collo-cygni(XP 023630050.1)
Antarctomyces psychrotrophicus isoform1a
Sclerotinia borealis(ESZ99258.1)
Rutstroemia sp.(PQE19745.1)
Pseudogymnoascus sp.(KFZ19926.1)
Rosellinia necatrix(GAP88793.1)
Chloromonas brevispina(AIC65768.1)
Streptomyces rishiriensis(WP 109003426.1)
Streptomyces niveus(WP 051433936.1)
Kitasatospora aureofaciens(OEV33719.1)
Amycolatopsis antarctica(WP 094864822.1)
Trichoderma harzianum(PKK41115.1)
Tolypocladium ophioglossoides(KND88274.1)
Alkalibacter saccharofermentans(WP 084117130.1)
Nocardioides psychrotolerans(WP 091113930.1)
Singulisphaera acidiphila(AGA28501.1)
Antarctomyces psychrotrophicus isoform2
Paludisphaera borealis(WP 076349425.1)
Paraburkholderia xenovorans(WP 011490876.1)
Psychroflexus torquis(AFU68394.1)
Flavobacteriaceae bacterium 3519-10 a(WP 012782099.1)
Euplotes focardii-derived bacterium a(AHG59377.1)
Flavobacteriaceae bacterium 3519-10 b(WP 012782099.1)
Euplotes focardii-derived bacterium b(AHG59377.1)
0.2
Group 1
Group 2
Group 3a
Group 3b

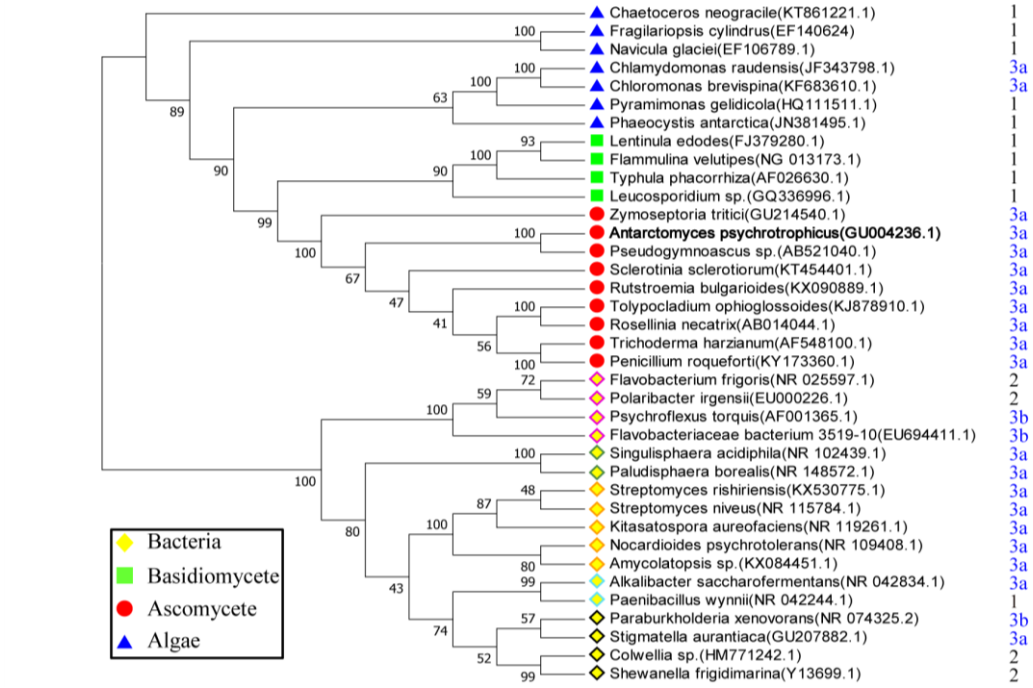
B
Chaetoceros neogracile(KT861221.1) 1
Fragilariopsis cylindrus(EF140624) 1
Navicula glaciei(EF106789.1) 1
Chlamydomonas raudensis(JF343798.1) 3a
Chloromonas brevispina(KF683610.1) 3a
Pyramimonas gelidicola(HQ111511.1) 1
Phaeocystis antarctica(JN381495.1) 1
Lentinula edodes(FJ379280.1) 1
Flammulina velutipes(NG 013173.1) 1
Typhula phacorrhiza(AF026630.1) 1
Leucosporidium sp.(GQ336996.1) 1
Zymoseptoria tritici(GU214540.1) 3a
Antarctomyces psychrotrophicus(GU004236.1) 3a
Pseudogymnoascus sp.(AB521040.1) 3a
Sclerotinia sclerotiorum(KT454401.1) 3a
Rutstroemia bulgarioides(KX090889.1) 3a
Tolypocladium ophioglossoides(KJ878910.1) 3a
Rosellinia necatrix(AB014044.1) 3a
Trichoderma harzianum(AF548100.1) 3a
Penicillium roqueforti(KY173360.1) 3a
Flavobacterium frigoris(NR 025597.1) 2
Polaribacter irgensii(EU000226.1) 2
Psychroflexus torquis(AF001365.1) 3b
Flavobacteriaceae bacterium 3519-10(EU694411.1) 3b
Singulisphaera acidiphila(NR 102439.1) 3a
Paludisphaera borealis(NR 148572.1) 3a
Streptomyces rishiriensis(KX530775.1) 3a
Streptomyces niveus(NR 115784.1) 3a
Kitasatospora aureofaciens(NR 119261.1) 3a
Nocardioides psychrotolerans(NR 109408.1) 3a
Amycolatopsis sp.(KX084451.1) 3a
Alkalibacter saccharofermentans(NR 042834.1) 3a
Paenibacillus wynnii(NR 042244.1) 1
Paraburkholderia xenovorans(NR 074325.2) 3b
Stigmatella aurantiaca(GU207882.1) 3a
Colwellia sp.(HM771242.1) 2
Shewanella frigidimarina(Y13699.1) 2
Bacteria
Basidiomycete
Ascomycete
Algae

Figure 2.4. Phylogenetic discrepancy between microbial 16S or 18S ribosomal RNA and DUF3494s. (A) Maximum likelihood tree based on the amino acid sequences of microbial DUF3494. The sequences confirmed to show ice-binding activity are underlined. (B) Neighbor phylogenetic tree of 16S or 18S ribosomal RNA of microorganisms. In both the figures, the numbers at the nodes indicate the bootstrap values for 500 replications (<30 are not shown), and the grouping (as in Fig. 3) is shown on the right side. In the DUF3494 tree, bootstrap values by ML and BI methods were shown as black and red, respectively. The edge colors of the bacterial and the algae markers indicate bacterial phyla as Proteobacteria (black), Planctomycetes (green), Firmicutes (cyan), Actinobacteria (orange), Bacteroidetes (purple), and unidentified (yellow) for bacteria, and *Bacillariophyta* (Black), *Haptophyta* (pink), and *Chlorophyta* (green) for algae.

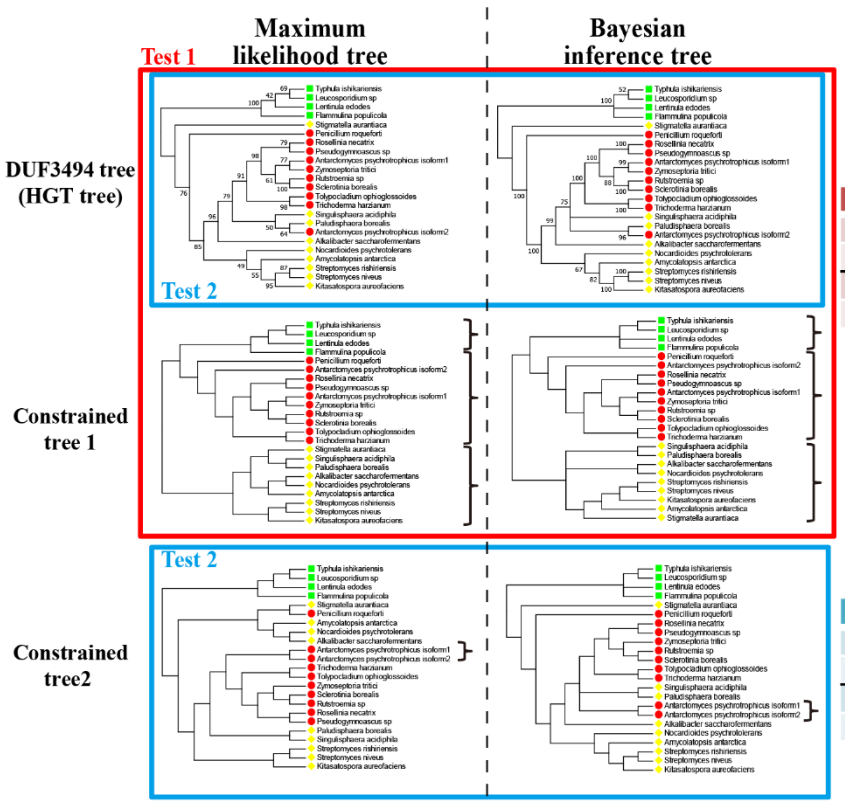

Test 1	AU	SH
HGT ML	0.985	1.000
Con ML	0.016	0.018
HGT Bay	0.994	1.000
Con Bay	0.006	0.008

Test 2	AU	SH
HGT ML	0.988	1.000
Con ML	0.000	0.002
HGT Bay	0.889	1.0000
Con Bay	0.000	0.000

Figure 2.5. Statistical tests performed on the phylogenetic trees prepared from the DUF3494 sequences and the host species. AU and SH tests of HGT tree against constrained tree in which ascomycetes, basidiomycetes, and bacteria form different clades (Red box). AU and SH tests of HGT tree against constrained tree in which AnpIBP isoforms are monophyly (Blue boxes). For the tree construction, ML (left

column) and BI (right column) methods were used. AU and SH test p-values are shown in right side tables. Bootstrap values for 500 replications are shown at the nodes. Markers are same as in Fig. 4.

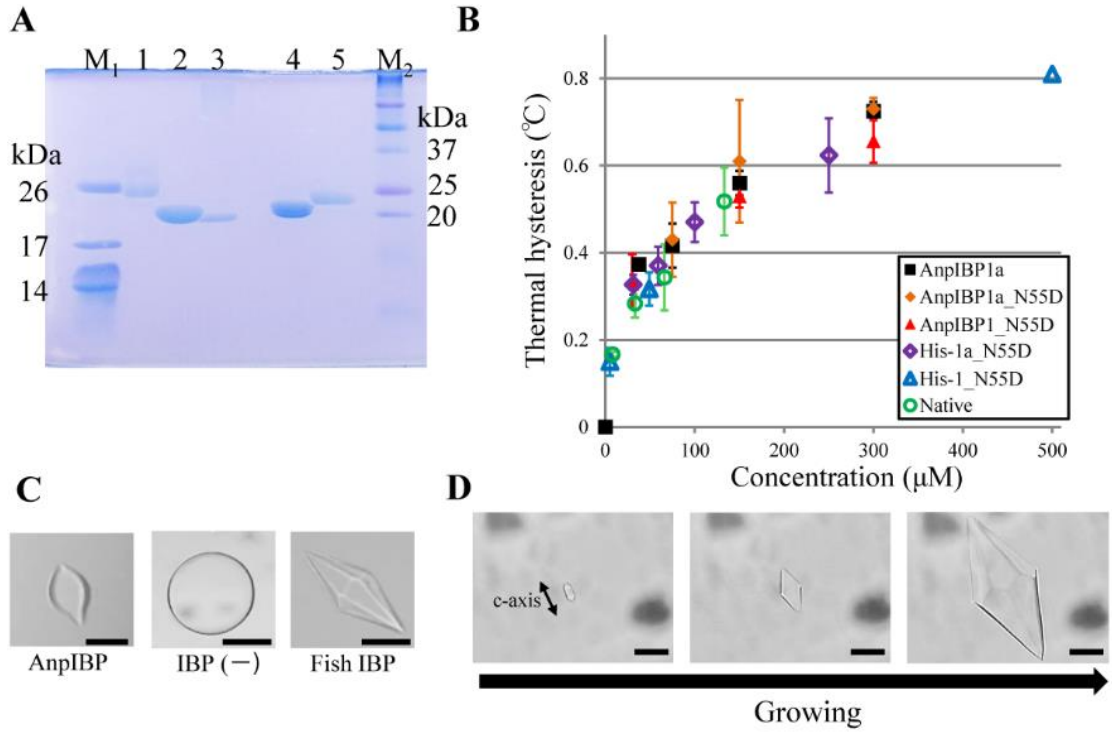

Figure 2.6. SDS-PAGE, TH activities, and ice crystal morphologies of recombinant AnpIBP1. (A) SDS-PAGE of purified AnpIBP1a and its mutants. M: Molecular weight marker; Lane 1, AnpIBP1a; Lane 2, AnpIBP1a N55D; Lane 3, AnpIBP1 N55D; Lane 4, His-tagged AnpIBP1 N55D; Lane 5, native AnpIBP. (B) The TH activity of AnpIBP and its mutants. Error bars indicate standard deviations of three times replications for three trials. (C) The comparison of ice crystal shapes in the IBP solution. Single ice-crystals formed in the presence and absence of IBPs were observed within TH gap. Scale bar = 25 μm. (D) Ice crystal morphology of AnpIBP1a. A single ice-crystal in AnpIBP1a solution was grown within TH (left panel) and below the freezing point (middle and right panels). The black arrow indicates the c-axis direction. Scale bar = 50 μm. These images were captured with a LEICA DMLB100 photomicroscope (Leica Microsystems, Wetzlar, Germany) equipped with a Linkam THMS 600 temperature controller (Linkam Scientific Instruments Ltd, Tadworth, Surrey, UK).

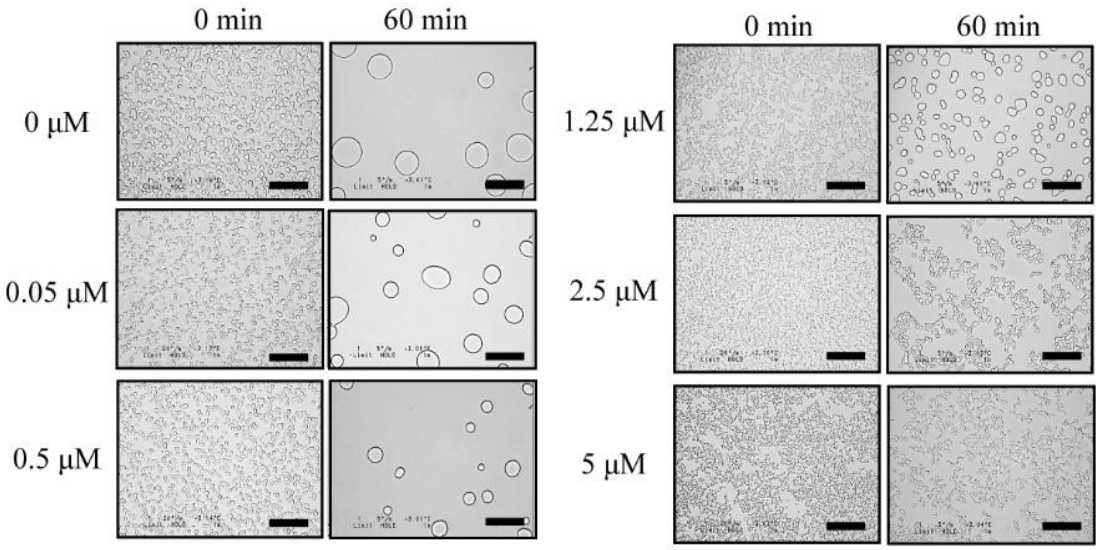

Figure 2.7. Concentration-dependence of IRI activity of AnpIBP1a. IBP concentration-dependent ice crystal morphologies before and after −3°C incubation. Ice crystals were observed under a photomicroscope. Scale bar = 50 μm.

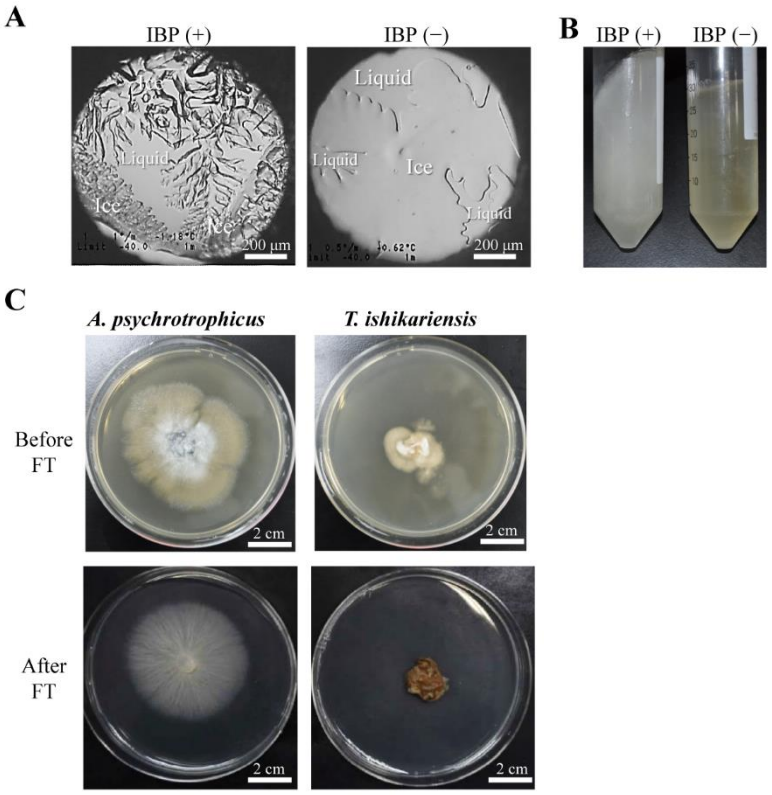

Figure 2.8. Effect of AnpIBP on ice crystal growth. (A) Microscopic view of ice

crystal growth in PDB medium with or without native AnpIBP. In IBP (+) medium, *A. psychrotrophicus* was cultured at 4°C for 1 month. In the *A. psychrotrophicus* culture, the size of the ice crystals was smaller than that in pure PDB medium. (B) Comparison of frozen PDB medium with or without AnpIBP. Formed ice was opaque in the presence of AnpIBP, whereas pure PDB medium was frozen as semi-transparent ice. (C) Mycelium growth on PDA plates of *A. psychrotrophicus* and *T. ishikariensis* with and without 25 cycles of freezing–thawing. *A. psychrotrophicus* is on the left side, and *T. ishikariensis* is on the right side.

Table 2.1. Sequence identities (%) between selected microbial DUF3494s. The sequences used here are the same as those used for the phylogenetic analysis (mentioned in Fig. 4A). Rows of bacteria, algae, basidiomycetes, and ascomycetes are indicated in yellow, blue, green, and red, respectively. The grouping is the same as in Fig. 3.

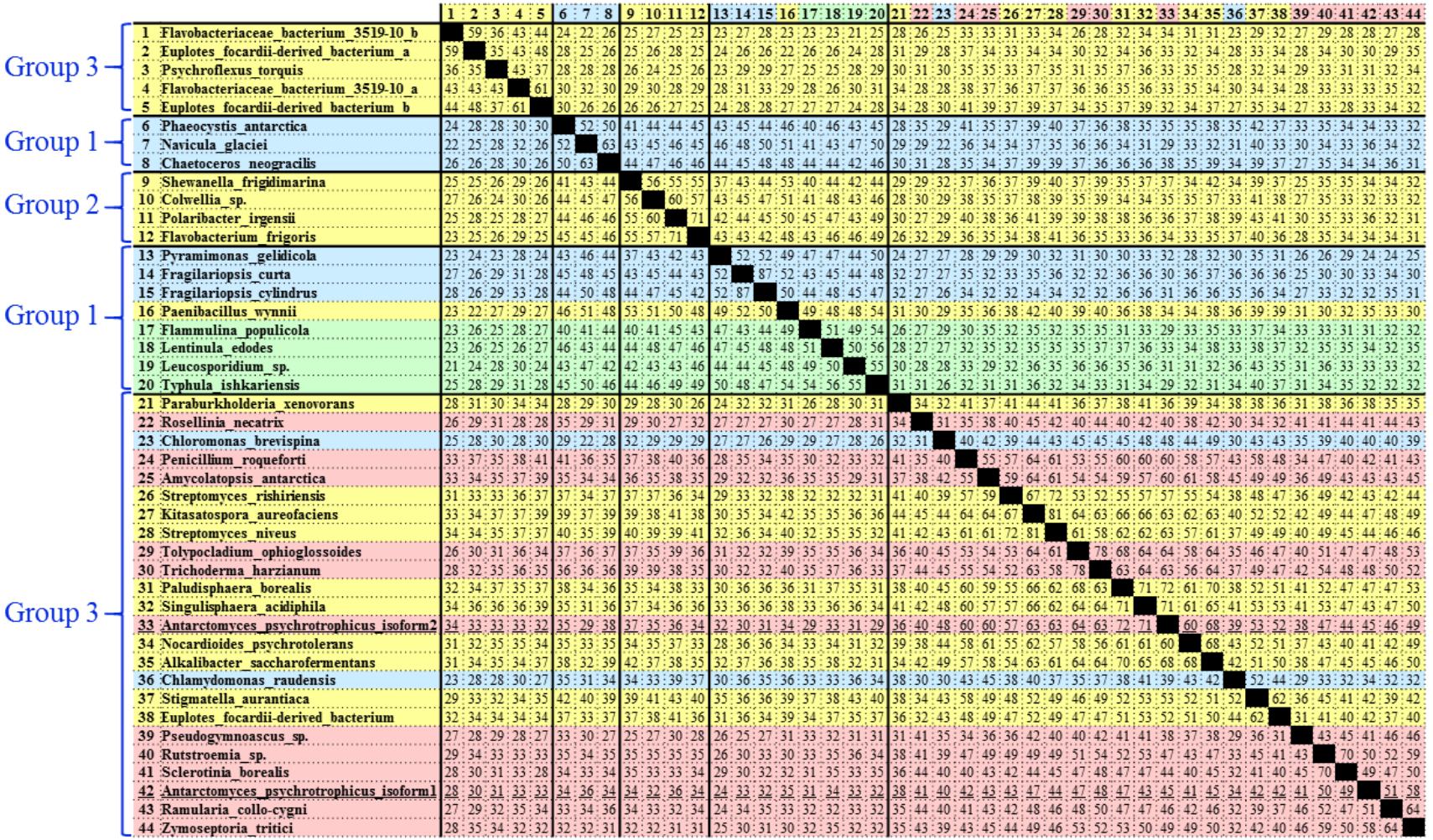
Group 3
Group 1
Group 2
Group 1
Group 3

2.6. References

1. Wang M, Tian J, Xiang M, & Liu X (2017) Living strategy of cold-adapted fungi with the reference to several representative species. *Mycology* **8**, 178–188.
2. De Maayer P, Anderson D, Cary C & Cowan DA (2014) Some like it cold: understanding the survival strategies of psychrophiles. *EMBO Rep* **15**, 508–517.
3. Su Y, Jiang X, Wu W, Wang M, Hamid MI, Xiang M & Liu X (2016) Genomic, transcriptomic, and proteomic analysis provide insights into the cold adaptation mechanism of the obligate psychrophilic fungus *Mrakia psychrophila*. *G3 Bethesda* **6**, 3603–3613.
4. Phadtare S (2004) Recent developments in bacterial cold-shock response. *Curr Issues Mol Biol* **6**, 125-136.
5. Duman JG & Olsen TM (1993) Thermal hysteresis protein activity in bacteria, fungi, and phylogenetically diverse plants. *Cryobiology* **30**, 322–328.
6. Davies PL (2014) Ice-binding proteins: a remarkable diversity of structures for stopping and starting ice growth. *Trends Biochem Sci* **39**, 548–555.
7. Knight CA, Hallett J & DeVries AL (1988) Solute effects on ice recrystallization: an assessment technique. *Cryobiology* **25**, 55–60.
8. Janech MG, Krell A, Mock T, Kang JS & Raymond JA (2006) Ice-binding proteins from sea ice diatoms (Bacillariophyceae). *J Phycol* **42**, 410–416.
9. Raymond JA & DeVries AL (1977) Adsorption inhibition as a mechanism of freezing resistance in polar fishes. *Proc Natl Acad Sci USA* **74**, 2589–2593.
10. Sun X, Griffith M, Pasternak JJ & Glick BR (1995) Low temperature growth, freezing survival, and production of antifreeze protein by the plant growth promoting rhizobacterium *Pseudomonas putida* GR12-2. *Can J Microbiol* **41**, 776–784.
11. Lee JK, Park KS, Park S, Park H, Song YH, Kang SH & Kim HJ (2010) An extracellular ice-binding glycoprotein from an Arctic psychrophilic yeast. *Cryobiology* **60**, 222–228.
12. Raymond JA & Janech MG (2009) Ice-binding proteins from enoki and shiitake mushrooms. *Cryobiology* **58**, 151–156.
13. Kiko R (2010) Acquisition of freeze protection in a sea-ice crustacean through horizontal gene transfer? *Polar Biol* **33**, 543–556.
14. Lee JH, Park AK, Do H, Park KS, Moh SH, Chi YM & Kim HJ (2012) Structural basis for antifreeze activity of ice-binding protein from arctic yeast. *J Biol Chem* **287**, 11460–11468.

15. Hoshino T, Kiriaki M, Ohgiya S, Fujiwara M, Kondo H, Nishimiya Y, Yumoto I & Tsuda S (2003) Antifreeze proteins from snow mold fungi. *Canad J Bot* **81**, 1175–1181.
16. Jones D & Sneath PH (1970). Genetic transfer and bacterial taxonomy. *Bacteriol Rev* **34**, 40–81.
17. Fitzpatrick DA (2012) Horizontal gene transfer in fungi. *FEMS Microbiol Lett* **329**, 1–8.
18. Bayer-Giraldi M, Uhlig C, John U, Mock T & Valentin K (2010) Antifreeze proteins in polar sea ice diatoms: diversity and gene expression in the genus *Fragilariopsis*. *Environ Microbiol* **12**, 1041–1052.
19. Raymond JA & Kim HJ (2012) Possible role of horizontal gene transfer in the colonization of sea ice by algae. *PloS one* **7**, e35968.
20. Raymond JA (2014) The ice-binding proteins of a snow alga, *Chloromonas brevispina*: probable acquisition by horizontal gene transfer. *Extremophiles* **18**, 987–994.
21. Xiao N, Suzuki K, Nishimiya Y, Kondo H, Miura A, Tsuda S & Hoshino T (2010) Comparison of functional properties of two fungal antifreeze proteins from *Antarctomyces psychrotrophicus* and *Typhula ishikariensis*. *FEBS J* **277**, 394–403.
22. Stchigel AM, Josep CANO, Mac Cormack W & Guarro J (2001) *Antarctomyces psychrotrophicus* gen. et sp. nov., a new ascomycete from Antarctica. *Mycol Res* **105**, 377-382.
23. Gonçalves VN, Vaz AB, Rosa CA & Rosa LH (2012) Diversity and distribution of fungal communities in lakes of Antarctica. *FEMS Microbiol Ecol* **82,** 459–471.
24. Loque CP, Medeiros AO, Pellizzari FM, Oliveira EC, Rosa CA & Rosa LH (2010) Fungal community associated with marine macroalgae from Antarctica. *Polar Biol* **33**, 641–648.
25. Graether SP, Kuiper MJ, Gagné SM, Walker VK, Jia Z, Sykes BD & Davies PL (2000). β-Helix structure and ice-binding properties of a hyperactive antifreeze protein from an insect. *Nature* **406**, 325–328.
26. Garnham CP, Campbell RL & Davies PL (2011) Anchored clathrate waters bind antifreeze proteins to ice. *Proc Natl Acad Sci USA* **108**, 7363–7367.
27. Park KS, Do H, Lee JH, Park SI, jung Kim E, Kim SJ, Kang SH & Kim HJ (2012) Characterization of the ice-binding protein from Arctic yeast *Leucosporidium* sp. AY30. *Cryobiology* **64**, 286–296.
28. Do H, Kim SJ, Kim HJ & Lee JH (2014) Structure-based characterization and antifreeze properties of a hyperactive ice-binding protein from the Antarctic

bacterium *Flavobacterium frigoris* PS1. *Acta Crystallogr D Biol Crystallogr* **70**, 1061–1073.

29. Sorhannus U (2011) Evolution of antifreeze protein genes in the diatom genus Fragilariopsis: evidence for horizontal gene transfer, gene duplication and episodic diversifying selection. *Evol Bioinform* **7**, 279–289.
30. Raymond JA & Morgan-Kiss R (2013) Separate origins of ice-binding proteins in Antarctic *Chlamydomonas* species. *PLoS One* **8**, e59186.
31. Pucciarelli S, Chiappori F, Devaraj RR, Yang G, Yu T, Ballarini P & Miceli C (2014). Identification and analysis of two sequences encoding ice-binding proteins obtained from a putative bacterial symbiont of the psychrophilic Antarctic ciliate *Euplotes focardii*. *Antarct Sci* **26**, 491-501.
32. Scotter AJ, Marshall CB, Graham LA, Gilbert JA, Garnham CP & Davies PL (2006) The basis for hyperactivity of antifreeze proteins. *Cryobiology* **53**, 229–239.
33. Kawahara H, Takemura T & Obata H (2006) Function analysis and screening of antifreeze material from fungi. *Cryobio Cryotech* **52**, 151–155.
34. Gwak Y, Jung W, Lee Y, Kim JS, Kim CG, Ju JH & Jin E (2014). An intracellular antifreeze protein from an Antarctic microalga that responds to various environmental stresses. *FASEB J* **28**, 4924–4935.
35. Vance TD, Graham LA & Davies PL (2018) An ice-binding and tandem beta-sandwich domain-containing protein in *Shewanella frigidimarina* is a potential new type of ice adhesin. *FEBS J* **285**, 1511-1527.
36. Guo S, Garnham CP, Whitney JC, Graham LA & Davies PL (2012) Re-evaluation of a bacterial antifreeze protein as an adhesin with ice-binding activity. *PloS one* **7**, e48805.
37. Martínez-Rosales C, Fullana N, Musto H & Castro-Sowinski S (2012) Antarctic DNA moving forward: genomic plasticity and biotechnological potential. *FEMS Microbiol Lett* **331**, 1–9.
38. Grabherr MG, Haas BJ, Yassour M, Levin JZ, Thompson DA, Amit I, Adiconis X, Fan L, Raychowdhury R, Zeng Q, Chen Z, Mauceli E, Hacohen N, Gnirke A, Rhind N, di Palma F, Birren BW, Nusbaum C, Lindblad-Toh K, Friedman N & Regev A (2011) Full-length transcriptome assembly from RNA-Seq data without a reference genome. *Nat Biotechnol* **29**, 644-652
39. Al-Samarrai TH & Schmid J (2000) A simple method for extraction of fungal genomic DNA. *Lett Appl Microbiol* **30**, 53–56.

40. Whelan S & Goldman N (2001) A general empirical model of protein evolution derived from multiple protein families using a maximum-likelihood approach. *Mol Biol Evol* **18**, 691-699.
41. Tamura K & Nei M (1993) Estimation of the number of nucleotide substitutions in the control region of mitochondrial DNA in humans and chimpanzees. *Mol. Biol. Evol* **10**, 512-526.
42. Shimodaira H (2002) An approximately unbiased test of phylogenetic tree selection. *Syst Biol* **51**, 492-508.
43. Shimodaira H & Hasegawa M (1999) Multiple comparisons of log-likelihoods with applications to phylogenetic inference. *Mol Biol Evol* **16**, 1114-1116.
44. Takamichi M, Nishimiya Y, Miura A & Tsuda S (2007) Effect of annealing time of an ice crystal on the activity of type III antifreeze protein. *FEBS J* **274**, 6469–6476.

Chapter 3 General Discussion

Ice-binding proteins, or antifreeze proteins, were firstly found in 1960s. After that, IBPs have been identified from various kinds of cold-adapted organisms such as fish, insects, plants, bacteria, yeast, and mushrooms. IBPs are thought to contribute to survival of these organisms. Many researchers have been involved in working on these proteins because of their unusual ligands (frozen water molecules), their incredible structural diversity, and their unique evolutionary history.

Previously, out group has reported that an Antarctic ascomycete *Antarctomyces psychrotrophicus* also produces IBP (AnpIBP), while its DNA and amino-acid sequences were not clarified. In Chapter 2, the author advanced this study and succeeded to identify three AnpIBP isoforms from the ascomycete and analyzed their evolutionary history and biophysical property. The main findings are the follows.

I. Three isoforms of AnpIBP were identified by total cDNA analysis of *A. psychrotrophicus*. Two of three mRNA sequences are highly transcribed in the ascomycete body at low temperature while they are not at 15°C, suggesting their importance at low temperature.
II. Two of the three mRNA of AnpIBP is made from one gene by alternative splicing, so that three mRNA sequences of AnpIBPs are transcribed from two genes in the genome of *A. psychrotrophicus*. We assume that alternative splicing of C-terminal non-IBP region in AnpIBP1 should have some roles. The C-terminal tail of AnpIBP1a has regularly spaced negative-charged residues, while AnpIBP1b have positively charged residues. In the current study, only AnpIBP1a was recombinantly expressed. To understand biophysical meaning of existence of the two AnpIBP1, expression of AnpIBP1b and further study are needed.
III. Phylogenetic analysis revealed that AnpIBP sequences are phylogenetically far from basidiomycete IBPs but close to bacterial IBPs, suggesting HGT of IBP genes from bacteria to ascomycetes. The most interesting finding is that *A. psychrotrophicus* has independently acquired these two IBP genes from two different bacteria. This unusual phenomenon strongly indicates the significance of IBP genes in cold regions such as Antarctica. The author has documented evidences and possible mechanisms of this observation, and have proposed that ascomycetes and bacteria frequently exchange the IBP genes, so as to colonize in the various icy environments. In the current study, ascomycete DUF3494 sequences that are only deposited in database were assumed to be IBPs. However, because of lack of study about ascomycete IBPs, it is still unclear whether these sequences are IBP or not.

IV. Mass preparation method of recombinant AnpIBP1a was successfully developed and its yield was about 200 mg/ 1L culture.

V. Recombinant AnpIBP1a showed both moderate TH and effective IRI activities, which is almost same as those of native IBP purified from culture supernatant of *A. psychrotrophicus*. Recombinantly expressed AnpIBP1a shows moderate TH activity and modifies a single ice-crystal into a unique rounded lemon shape. To understand this unique ice-plane affinity, molecular ice-binding mechanism of AnpIBP1a is needed.

Acknowledgements

First, I would like to sincerely thank my supervisor, Dr. Sakae Tsuda, for his kind, patient and considerate advice. I have learned many things from him. He often says “Think about how to explain your study to a high school student”, “Good figure makes good paper”, “Make the audiences understanding is the most important, and preciseness is the second”. Thanks to such words, I made significant progress as a scientist. Dr. Tsuda is an excellent scientist. It has been my pleasure to work and study under his guidance. And also, I thank Dr. Hidemasa Kondo, for discussion, technical guidance, and providing pointed advice.I am also very thankful to everybody in the Tsuda lab, past and present. I would like to thank Dr. Mami Sakashita, Dr. Yoshiyuki Nishimiya and Dr. Tamotsu Hoshino for their helpful technical assistance and guidance. I would also like to thank Mrs. Ai Miura for her fundamental supports for years. I am also very grateful to all students in this lab for their accompanying, supporting and encouraging every day.